

Journal Pre-proofs

Comprehensive multi-omics analyses exposes a precision therapy strategy that targets replication stress in hepatocellular carcinoma using WEE1 inhibition

Xing Jia, Xingxin Zhu, Shinuo Chen, Qiongzi Qiu, Wenfeng Song, Shiyu Zhang, Haijiang Dong, Zequn Li, Suchen Bian, Hao Wu, Haojiang Dai, Cheng Jin, Mengqiao Zhou, Chen Jun, Zefeng Xuan, Pengfei Liu, Qiufang Zeng, Haiyang Xie, Shusen Zheng, Penghong Song

PII: S2090-1232(25)00114-6
DOI: <https://doi.org/10.1016/j.jare.2025.02.016>
Reference: JARE 2029

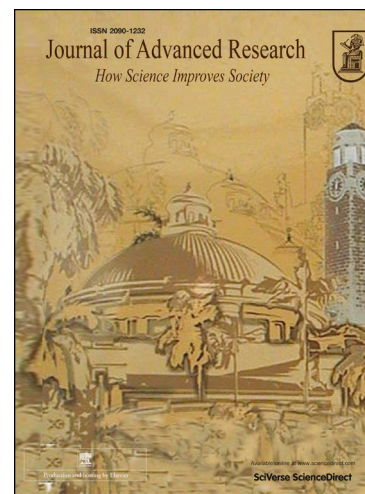
To appear in: *Journal of Advanced Research*

Received Date: 31 July 2024
Revised Date: 10 February 2025
Accepted Date: 11 February 2025

Please cite this article as: Jia, X., Zhu, X., Chen, S., Qiu, Q., Song, W., Zhang, S., Dong, H., Li, Z., Bian, S., Wu, H., Dai, H., Jin, C., Zhou, M., Jun, C., Xuan, Z., Liu, P., Zeng, Q., Xie, H., Zheng, S., Song, P., Comprehensive multi-omics analyses exposes a precision therapy strategy that targets replication stress in hepatocellular carcinoma using WEE1 inhibition, *Journal of Advanced Research* (2025), doi: <https://doi.org/10.1016/j.jare.2025.02.016>

This is a PDF file of an article that has undergone enhancements after acceptance, such as the addition of a cover page and metadata, and formatting for readability, but it is not yet the definitive version of record. This version will undergo additional copyediting, typesetting and review before it is published in its final form, but we are providing this version to give early visibility of the article. Please note that, during the production process, errors may be discovered which could affect the content, and all legal disclaimers that apply to the journal pertain.

© 2025 Published by Elsevier B.V. on behalf of Cairo University.



Title Page

Title: Comprehensive Multi-omics Analyses Exposes a Precision Therapy Strategy that Targets Replication Stress in Hepatocellular Carcinoma Using WEE1 Inhibition.

Authors

Xing Jia^{2,3,4,5#}, **Xingxin Zhu**^{1,3,4,5#}, **Shinuo Chen**^{1,3,4,5#}, Qiongzi Qiu⁶, Wenfeng Song^{1,3,4,5}, Shiyu Zhang^{1,3,4,5}, Haijiang Dong⁷, Zequn Li^{1,3,4,5}, Suchen Bian^{1,3,4,5}, Hao Wu^{1,3,4,5}, Haojiang Dai^{1,3,4,5}, Cheng Jin^{1,3,4,5}, Mengqiao Zhou^{1,3,4,5}, Chen Jun^{1,3,4,5}, Zefeng Xuan^{1,3,4,5}, Pengfei Liu⁸, Qiufang Zeng⁸, Haiyang Xie^{1,3,4,5}, **Shusen Zheng**^{1,3,4,5,9*}, and **Penghong Song**^{1,3,4,5,10*}

Affiliations

1. Division of Hepatobiliary and Pancreatic Surgery, Department of Surgery, The First Affiliated Hospital, Zhejiang University School of Medicine, Hangzhou 310003, China
2. Thyroid Surgery Department, Zhejiang Cancer Hospital, Hangzhou 310022, Zhejiang, China.
3. NHC Key Laboratory of Combined Multi-organ Transplantation, Hangzhou 310003, China
4. Key Laboratory of the Diagnosis and Treatment of Organ Transplantation, Research Unit of Collaborative Diagnosis and Treatment for Hepatobiliary and Pancreatic Cancer, Chinese Academy of Medical Sciences (2019RU019), Hangzhou 310003, China
5. Key Laboratory of Organ Transplantation, Research Center for Diagnosis and Treatment of Hepatobiliary Diseases, Zhejiang Province, Hangzhou 310003, China
6. Center for Uterine Cancer Diagnosis & Therapy Research of Zhejiang Province, Women's Reproductive Health Key Laboratory of Zhejiang Province, and Department of Gynecologic Oncology, Women's Hospital, Zhejiang University School of Medicine, Hangzhou, 310029, Zhejiang, China.
7. The First Affiliated Hospital of Zhengzhou University, Zhengzhou, 450052, Henan, China.
8. Shanghai Applied Protein Technology Co. Ltd, Shanghai, 200000, China.

9. Department of Hepatobiliary and Pancreatic Surgery, Shulan (Hangzhou) Hospital, Hangzhou 310003, Zhejiang, China.

10. State Key Laboratory for Diagnosis and Treatment of Infectious Diseases, First Affiliated Hospital, Zhejiang University School of Medicine, Hangzhou 310003, China

#These authors contributed equally to this work.

***Corresponding author:** Penghong Song, The First Affiliated Hospital Zhejiang University, 79 Qingchun Road, Hangzhou 310003, China, Email: songpenghong@zju.edu.cn; and Shusen Zheng, The First Affiliated Hospital Zhejiang University, 79 Qingchun Road, Hangzhou 310003, China, E-mail: shusenzheng@zju.edu.cn.

Credit author statement:

Xing Jia: Conceptualization, Methodology, Validation, Investigation, Writing - Original Draft; **Xingxin Zhu:** Conceptualization, Methodology, Validation, Writing - Original Draft; **Shinuo Chen:** Conceptualization, Methodology, Validation, Writing - Original Draft; **Qiongzi Qiu:** Software, Data Curation, Visualization; **Wenfeng Song:** Data Curation, Resources, Visualization; **Shiyu Zhang:** Conceptualization, Methodology; **Haijiang Dong:** Data Curation, Resources; **Zejun Li:** Investigation, Validation; **Suchen Bian:** Investigation, Validation; **Hao Wu:** Investigation, Validation; **Haojiang Dai:** Investigation, Validation; **Cheng Jin:** Investigation, Validation; **Mengqiao Zhou:** Investigation, Validation; **Chen Jun:** Funding acquisition; **Zefeng Xuan:** Funding acquisition; **Pengfei Liu:** Software; **Qiufang Zeng:** Software; **Haiyang Xie:** Conceptualization, Supervision, Funding acquisition; **Shusen Zheng:** Conceptualization, Writing - Review & Editing, Supervision, Funding acquisition; **Penghong Song:** Conceptualization, Writing - Review & Editing, Supervision, Funding acquisition.

Competing interest Statement

The authors declare that they have no competing interests.

Funding

This study was supported by grants from the National Natural Science Foundation of China (No. 82070652, No. 81870434), the Key Research and Development Plan of Zhejiang Province (No.

2020C04003), Zhejiang Provincial Natural Science Foundation of China (LQ21H030006), Exploration Project of Zhejiang Natural Science Foundation (LQ22H160031), Research Unit Project of the Chinese Academy of Medical Sciences (2019-I2M-5-030), the Research Project of Jinan Microecological Biomedicine Shandong Laboratory (JNL-2022007B), and the State Key Laboratory for Diagnosis and Treatment of Infectious Diseases (zz202302).

Keywords: Multi-omics; Replication stress; Adavosertib; Oxaliplatin; Precision medicine; Hepatocellular carcinoma.

Title

Comprehensive Multi-omics Analyses Exposes a Precision Therapy Strategy that Targets Replication Stress in Hepatocellular Carcinoma Using WEE1 Inhibition.

Abstract

Introduction:

Hepatocellular carcinoma (HCC) is an extremely heterogeneous malignancy with a poor prognosis, highlighting the need to target specific vulnerabilities within the tumor during treatment.

Objectives:

This study employs multi-omics analysis techniques to provide novel insights into personalized therapeutic strategies for HCC patients.

Methods:

We performed proteomic and transcriptomic sequencing on 178 and 94 clinical samples of primary HCC without prior treatment, respectively. We employed an unbiased Kinome CRISPR-Cas9 library screening approach to systematically evaluate and identify novel therapeutic strategies that specifically target replication stress (RS). The synergy between oxaliplatin and adavosertib was verified using *in vitro* and *in vivo* models, including hydrodynamic injection, patient-derived organoids, and patient-derived xenografts.

Results:

In both proteomic- and transcriptomic-based subtyping analyses, subtypes characterized by hyperproliferative features demonstrated the poorest prognosis and the highest levels of RS. Among all first-line chemotherapeutic agents in these analyses, oxaliplatin accumulated the highest RS levels in HCC, while resistance remained a major challenge. With unbiased Kinome CRISPR loss-of-function gene screening, WEE1 was identified as a synthetic lethal target of oxaliplatin. The synergy between the WEE1 inhibitor adavosertib and oxaliplatin has been demonstrated in multiple *in vitro* and *in vivo* models. Mechanistically, adavosertib inhibits oxaliplatin-induced homologous recombination repair and G2/M checkpoint activation, leading to the accumulation of lethal DNA

damage. Furthermore, patients with HCC showing high RS levels had poor prognoses and responded well to adavosertib and oxaliplatin combination treatments. This was validated by preclinical models and unsupervised clustering analysis.

Conclusions:

Our findings provide promising insights into the precise therapeutic targeting of RS in HCC at both the proteomic and transcriptomic levels. Furthermore, our study highlights the potential of combining oxaliplatin with adavosertib as a treatment approach for HCC.

Significance Statement

In this study, we analyzed 178 and 94 pairs of clinical HCC samples using proteomic and transcriptomic sequencing, respectively. We discovered that the subtype characterized by high proliferation had the worst prognosis and highest RS level. Drug screening revealed that oxaliplatin promotes RS accumulation in HCC, but its resistance remains a challenge. Through unbiased CRISPR deletion-gene screening, WEE1 was identified as a lethal target of oxaliplatin. The WEE1 inhibitor adavosertib inhibits oxaliplatin-induced DNA repair, leading to lethal DNA damage accumulation. Furthermore, our clustering analysis based on RS levels demonstrated that HCC patients with high RS levels have poorer prognoses and be more beneficial from adavosertib and oxaliplatin combination therapy. These findings support an individualized treatment approach for HCC targeting RS based on WEE1 Inhibition.

Introduction

Among all cancers, hepatocellular carcinoma (HCC) is the third leading cause of death from cancer worldwide^[1]. In early stage HCC, surgical treatment may be effective, but the five-year survival rate remains low^[2]. Over the past twenty years, large-scale multi-omics analyses, including proteomics and transcriptomics, revealed that HCC is highly heterogeneous^[3-5]. This suggests that standard therapeutic strategies are only efficacious for limited subtypes of patients. Therefore, there is an urgent need for more effective cancer vulnerability-targeting or individualized treatment strategies against advanced HCC.

Replication stress (RS) is closely linked to a defective DNA damage response (DDR), leading to genomic instability, which is a hallmark of cancer^[6]. Due to the higher RS level, cancer cells depend on enhanced RS response pathways, such as DDR and cell cycle checkpoint regulation for survival^[7]. Two approaches are being investigated for therapeutically targeting RS^[8,9]: 1) Inducing catastrophic DNA damage by overriding cell cycle checkpoints and 2) pushing cells with unresolved RS into the cell cycle by depleting cellular resources vital for DNA replication.

Oxaliplatin is a chemotherapeutic agent frequently used for advanced HCC^[10,11], and inhibits tumor cell proliferation by inducing DNA damage and exogenously increasing tumor cell RS. However, some patients are prone to oxaliplatin resistance and tumor recurrence^[12-14]. It is therefore urgent to find synthetic lethal targets that are more sensitive to oxaliplatin.

The protein kinase WEE1 inhibits cyclin-dependent kinases 1 and 2 (CDK1/2), causing the G2/M cell cycle checkpoint to activate, and cell cycle arrest to allow time for DNA repair^[15,16]. In recent studies, it has been suggested that tumor cells exhibiting high levels of RS or TP53 mutations may be more susceptible to DDR inhibitors, including WEE1 inhibitors^[17-19]. Adavosertib (AZD1775 or MK1775), a narrow-spectrum inhibitor of WEE1, has antitumor activity, either alone or in combination with chemotherapy, and has been studied in a number of Phase II clinical trials^[20-22]. Both preclinical and clinical data indicate that adavosertib causes DNA damage, accelerates mitotic entry, and when combined with chemotherapy, enhances antitumor efficacy^[23]. Nevertheless, the efficacy of adavosertib in targeting the vulnerability of RS in HCC remains to be investigated.

This study revealed that both proteomics and transcriptomics subgroups with over-proliferation exhibited the poorest prognoses and the highest RS levels in the cohort, suggesting the possibility of targeting RS for HCC treatment. Preclinical drug screening tests and unbiased kinome CRISPR

deletion-gene screening indicated that the combination of adavosertib and oxaliplatin may be the most effective treatment for RS in HCC. The combination of adavosertib and oxaliplatin enhanced DNA damage and induced mitotic catastrophe and apoptosis, resulting in an accumulation of RS with a consequent synergistic effect. These results indicate that this combination may offer potent antitumor effects by targeting RS in HCC. Furthermore, our findings suggest that tumor RS level could serve as a prognostic marker for HCC and guide drug treatment regime based on risk-benefit analysis, providing valuable insights for precision therapies.

Results

1. Classification of HCC based on proteomics and transcriptomic analysis

To gain a comprehensive molecular understanding of patients with HCC, paired non-tumor and tumor liver tissue samples were collected from 178 individuals diagnosed with HCC for proteogenomic analysis. An additional 94 patients were included in the study and paired tissue samples from these patients were evaluated according to strict transcriptomic analysis criteria (Fig. 1A).

Isobaric tandem mass tags (TMT)-based global proteomics identified 9,544 proteins, with a median of 7,653 proteins per sample (Fig. S1A-D and Table S1). Quality control (QC) analysis of the protein groups, which showed a high Spearman correlation coefficient, confirmed the high quality of the mass spectrometer (Fig. S1E). Proteomic data were analyzed using principal component analysis (PCA), revealing no obvious differences in the years of sample collection or experimental batches, suggesting the absence of batch effects (Fig. S1F, G). Furthermore, the PCA data demonstrated significant spatial separation between tumor and non-tumor tissues (Fig. S1H). The volcano plot and Kyoto encyclopedia of genes and genomes (KEGG) enrichment results based on differential genes between tumor and non-tumor tissues showed different expression patterns (Fig. S1I, J and Table S2, S3).

To evaluate the heterogeneity and homogeneity among tumor tissue samples, unsupervised clustering was conducted based on the coefficient of variation (CV top 95%) of proteins in the tissue samples using Nonnegative Matrix Factorization (NMF) (Fig. S1K and Fig. S2A-C). This analysis identified three subgroups (S-I, S-II, and S-III) among the 178 samples (Fig. 1B and Table S4, S5). PCA results identified a significant spatial separation specifically categorizing the tumor tissues into the three subgroups (Fig. S2D), as opposed to the paired non-tumor liver tissues (Fig. S2E). Notably, S-II exhibited higher levels of vascular invasion ($p = 0.0043$), recurrence rates ($p = 0.0491$), and TNM stages than the other two subgroups and had the worst prognosis (Fig. 1C, Fig. S2F, and Table S6). Different molecular profiles were found among the three proteomic subgroups based on pathway enrichment analyses (Fig. 1D). Features of S-II were more likely driven by proliferative signaling including epithelial-mesenchymal transition, E2F targets, G2/M checkpoint, mitotic spindle, KRAS targets, MYC targets, and others. The S-III subgroup exhibited high xenobiotic metabolism, peroxisome, adipogenesis, fatty acid metabolism, and others, indicating tumors of this

subgroup were possibly driven by elevated metabolic processes. A few pathways (E2F targets, G2/M checkpoint, and Peroxisome) were differentially activated in S-I, resembling a partial mixture of S-II and S-III features including intermediate activation of certain metabolic and proliferation-signaling pathways. In addition, Gene Ontology (GO) enrichment analysis results revealed significant enrichment of humoral immunity-related pathways in S-II subtype compared to S-I and S-III subtypes (Fig. S2G and Table S7). Tumors with highly proliferative tendencies tended to have high levels of RS, and further Gene Set Enrichment Analysis (GSEA) results indicated that S-II had higher RS levels compared to the other two subgroups (Fig. S2H).

For transcriptomic analysis and to define the molecular subgroups of HCC, we extracted 5,000 genes showing the highest expression variation in tumor tissues (adjusted p-value < 0.05, Wilcoxon test with Benjamini-Hochberg correction), based on RNA-seq data from 94 patients with primary HCC (Table S8). Consistency checks (Fig. S3A, B) and factorization rank assessments within clusters (Fig. S3C) showed that all 94 patients with HCC could be classified into three subgroups based on NMF: S-I, S-II, and S-III (Fig. 1E). Notably, S-III demonstrated significantly higher tumor sizes ($p = 0.0037$), recurrence rates ($p = 0.0081$) and TNM stages compared to the other two subgroups (Fig. 1E, Fig. S3D, and Table S9). Furthermore, the S-III subgroup had the worst prognosis (Fig. 1F). Molecular profiles of each transcriptomic subgroup were revealed through pathway enrichment analysis (Fig. 1G). The S-I subgroup exhibited the highest immune activation characteristics, such as B cell activation, CD4 positive alpha-beta T cell activation, T cell proliferation, regulation of macrophage activation, and others. Features of S-II were likely driven by metabolic processes such as long-chain fatty acid metabolic process, fatty acid transport, vitamin transport, serine family amino acid metabolic process, and others. Conversely, S-III exhibited high mitotic nuclear division, cell cycle checkpoint signaling, regulation of DNA repair, mitotic cytokinesis, and others, indicating that tumors in this subgroup are driven by increased proliferative processes. Additionally, GO enrichment analysis and GSEA results indicated that S-III had higher RS-related pathway activation than the other two subgroups (Fig. S3E, F and Table S10).

Subsequently, integrated analyses of proteomics and transcriptomics (Fig. S4A, B and Table S11) revealed a positive correlation trend between quantified proteins and their associated genes, with a correlation coefficient of 0.4819 (Fig. S4C). In addition, the correlation coefficient of differentially expressed proteins and genes compared with adjacent non-tumor tissues was 0.7629 (Fig. S4D), and the correlation coefficient of proteins/genes with the same trend was 0.8065 (Fig. S4E). Further pathway enrichment analysis of proteins and genes that exhibited the same trend demonstrated

significant activation of RS-related gene sets (Fig. S4F, G). In addition, we also analyzed the overlap between proteomic and transcriptomic samples (Fig. S4H) and examined the correspondence of patients classified by both modalities into transcriptomic subtypes and proteomic subtypes (Fig. S4I).

Notably, these results highlight that subgroups with high RS levels have significantly worse outcomes in both proteomic and transcriptomic typing analyses. Differential levels of RS in tumor tissues versus normal tissues were investigated using GSEA to assess RS-related gene sets. Our analyses revealed that these gene sets were upregulated in tumor tissues compared to normal tissues, based on proteomics data (Fig. S5A) and transcriptomics data cohort (Fig. S5B), and The Cancer Genome Atlas (TCGA) database (Fig. S5C). Gene Expression Profiling Interactive Analysis (GEPIA) analysis (<http://gepia.cancer-pku.cn/>) also revealed increased expression of DDR-related genes in HCC (Fig. S5D).

So far, our study has established a comprehensive subtyping landscape for HCC through proteomic and transcriptomic analyses. Additionally, our findings strongly support the notion that RS is indeed a distinct characteristic and a highly promising therapeutic target for HCC.

2. Drug screening identified oxaliplatin as a RS-targeting therapy for treating HCC

To examine the potential impact of targeting RS in HCC, we employed patient-derived xenograft (PDX) models of different proteomic subgroups to evaluate several chemotherapeutic agents commonly used for clinical gastrointestinal tumors (Fig. 2A): gemcitabine (100 mg/kg), oxaliplatin (10 mg/kg), epirubicin (3.5 mg/kg), 5-FU (50 mg/kg), irinotecan (15 mg/kg), and paclitaxel (10 mg/kg), as well as sorafenib (60 mg/kg), a first-line therapeutic agent for HCC [24]. The first-line chemotherapy agent, oxaliplatin, had the highest therapeutic effect on the PDX models (Fig. 2B and Fig. S6A-C), causing a significant increase in RS accumulation, shown by immunohistochemical (IHC) staining for p-RPA2 (S4/S8) (Fig. 2C). However, because many patients develop oxaliplatin resistance and tumor recurrence, identifying key molecules linked to oxaliplatin resistance and analyzing new treatment strategies remains critical^[25].

3. Identification of WEE1 as a synthetic lethal gene of oxaliplatin in HCC through kinome-targeted CRISPR/Cas9 library screening

Signal transduction is crucial for kinases, which are attractive targets for drugs^[26]. To systematically

identify sensitive synergistic targets of oxaliplatin treatment, a kinome-targeted CRISPR/Cas9 library-based negative selection approach^[27] was performed to screen for genes that, when deleted, potentiate the antitumor effects of oxaliplatin (Fig. 2H). The results of this screen identified WEE1 as the most significant synthetic lethal gene post-oxaliplatin treatment in Huh7 cells (Fig. 2D, E and Table S12). Previous studies have highlighted WEE1's regulatory role in CDK1 phosphorylation, activating the G2/M checkpoint, and RS response^[28, 29]. Western blots and IHC staining (n=113) demonstrated higher WEE1 expression in HCC tumors compared to adjacent non-tumor tissues (Fig. S6D and Fig. 2F). WEE1 and CDK1 mRNA expression levels were significantly higher in HCC tumors (Fig. 2G and Fig. S6E). The TCGA database showed that higher levels of WEE1 or CDK1 expression are associated with poorer survival outcomes (Fig. 2H and Fig. S6F). Additionally, the HCC subgroup with the highest RS, S-III had the highest WEE1 and CDK1 mRNA expression compared to the remaining two subgroups (Fig. S6G). Separate GSEA using the proteomics data (Fig. S6H), transcriptomics data (Fig. S6I), and TCGA database (Fig. S6J), revealed that the G2/M checkpoint gene set was upregulated in HCC tumor tissues compared to non-tumor tissues. Based on these findings, targeting WEE1 in HCC may be a promising approach to counteract RS and synthetic lethal genes.

4. Synergistic suppression of HCC malignant phenotypes by oxaliplatin and adavosertib *in vitro* and *in vivo*

The WEE1 inhibitor adavosertib (AZD1775 or MK1775) is currently in multiple phase II clinical trials (<http://www.clinicaltrials.gov>). In various HCC cell lines, adavosertib combined with oxaliplatin showed synergistic inhibition of cell viability when used alone or in combination. In most HCC cell lines, the combination treatment showed synergistic effects, as indicated by a combination index (CI) less than 1 (Fig. 3A). Additionally, the combination treatment decreased colony formation (Fig. 3B, C) and tumorsphere formation efficiency (Fig. 3D). The combination treatment of oxaliplatin and adavosertib was tested *in vivo* first by establishing xenograft models with Huh7 cells and treated mice with single-agent treatment (oxaliplatin (10 mg/kg) or adavosertib (50 mg/kg); combination treatment; or vehicle control). Combining oxaliplatin and adavosertib significantly suppressed tumor growth, consistent with *in vitro* experiments (Fig. 3E). Tumor weight and volume were significantly reduced, and no significant changes in mouse body weight were observed (Fig. 3F-H). In addition, orthotopic HCC models demonstrated that the combination treatment significantly suppressed tumor growth (Fig. 3I-K).

Moreover, we comprehensively assessed the impact of combining oxaliplatin and adavosertib against HCC progression. The combination treatment significantly reduced the migration and invasion of HCC cells according to transwell tests and wound healing assays (Fig. S7A-D). Cells treated with the combination showed a significant reduction in pseudopods, which are required for cell motility (Fig. S7E, F).

5. Adavosertib inhibits homologous recombination and synergistically enhances oxaliplatin-induced DNA damage in HCC cells

RNA-seq was used to detect transcriptional changes in oxaliplatin-treated and adavosertib-treated Huh7 cells compared to vehicle control (Fig. S8A-D). In this analysis, RS-related terms such as DNA damage, cell cycle checkpoint, and apoptosis were upregulated in both treatment groups. However, after oxaliplatin or adavosertib treatment, some genes associated with DNA damage repair had different expression trends, which could be a reason for the synergistic effect (Fig. S8E, F). Interestingly, we also found that both WEE1 expression and the G2/M checkpoints were significantly activated following oxaliplatin treatment (Fig. S8G, H).

GSEA indicated a significant enrichment of DDR-related genes after treatment with adavosertib or oxaliplatin (Fig. 4A). We validated this effect by utilizing comet tail assays (Fig. S9A) and measuring DNA damage-associated protein expression levels (Fig. 4B) in single-agent treated HCC cells, which increased in a dose-dependent manner. Importantly, combination therapy resulted in significantly higher levels of comet tail (Fig. 4C), γ H2AX foci (Fig. 4D), and DNA damage-associated protein expression levels (Fig. 4E), compared to single-agent treatments. This confirmed that the synergistic combination of adavosertib and oxaliplatin leads to an increase in double-strand breaks (DSBs) and replication fork collapse in HCC cells.

The RNA-seq data revealed that most DNA damage repair-related genes were activated after oxaliplatin treatment but repressed after adavosertib treatment (Fig. 4F and Table S13). In order to further explore the potential mechanism of adavosertib enhancing DNA damage, the pDR-GFP or pimeJ5-GFP reporting systems were used to investigate its effect on homologous recombination (HR) or non-homologous recombination repair (NHEJ), respectively. Results showed that adavosertib decreased HR-mediated DNA double-strand break repair efficiency in both SNU449 and Huh7 cells; whereas, increased NHEJ-mediated DNA repair efficiency, which was confirmed by examining HR-related and NHEJ-related proteins (Fig. 4G-J). Notably, nuclear RAD51 foci, an

HR marker that co-localized with γ H2AX foci, was significantly activated following oxaliplatin treatment, while adavosertib antagonized RAD51 activation in the combination group (Fig. 4K). In addition, the NHEJ marker 53BP1 was activated after drug treatments, but was more evident after adavosertib treatment (Fig. 4I). GSEA results supported our conclusion that adavosertib could counteract oxaliplatin-induced enhancement of HR repair activation while simultaneously promoting NHEJ DNA repair mechanisms (Fig. S9B, C).

6. Oxaliplatin in combination with adavosertib disrupts the cell cycle and excessive RS

After analyzing KEGG pathway enrichment and GSEA, significant alterations in the cell cycle were observed with both single-agent treatments (Fig. S10A, B and Fig. 5A). Oxaliplatin treatment prolonged S-phase occurrence and shortened the G2/M phase, activating G2/M checkpoint-related proteins and decreasing the expression of the mitotic-specific marker, p-HH3(S10), in HCC cells. In contrast, adavosertib led to G2/M checkpoint inactivation, driving a large proportion of cells into the M phase (Fig. S10C, D and Fig. 5B-D). Since WEE1 can prolong the S-phase and activate the G2/M cell-cycle checkpoint, which allows cells to repair DNA before mitosis [15], GSEA results further suggested that G2/M checkpoints were active after oxaliplatin treatment but deactivated after adavosertib treatment (Fig. 5E). Moreover, we examined the effect of the drug combination on the cell cycle and found that adavosertib partially reversed oxaliplatin-induced decrease of the G2/M cell ratio (Fig. 5F and Fig. S10E). Immunofluorescence labeling of p-HH3 confirmed Adavosertib increased mitotic cell numbers after oxaliplatin treatment partially (Fig. 5G). Additionally, western blot results revealed that while inhibitory phosphorylation of CDK1 and other G2/M checkpoint-associated proteins was elevated after oxaliplatin stimulation, combined treatment with adavosertib effectively abrogated this effect in SNU449 and Huh7 cells (Fig. 5H).

In previous studies, the ATR-CHK1-WEE1 axis has been demonstrated to be crucial for regulating the cell cycle response to RS^[30]. We observed that adavosertib treatment suppressed ATR activation in response to RS (Fig. S10F), and the combination treatment significantly increased RS accumulation in HCC cells, as evidenced by immunofluorescence staining of p-RPA2 (S4/S8) (Fig. 5I). Metaphase spread assay results indicated that the combination treatment generated significantly more chromosomal abnormalities than each monotherapy, underscoring an increased level of chromosomal instability (Fig. 5J). By suppressing oxaliplatin-induced DNA damage checkpoint activation, avosertib treatment led to cells entering mitosis without reparation of DNA damage. We found that cells treated by the combination had significantly more DNA damage at different stages

of mitosis compared to untreated and single-agent treated cells (Fig. 5K).

7. Combined treatment with oxaliplatin and adavosertib resulted in premature mitosis and synergistically triggered enhanced apoptosis in HCC cells

Chromosomal aberrations are frequently associated with catastrophic chromosomal events that are lethal to cancer cells^[31]. The mitotic morphology of HCC cells that received various drug treatments were evaluated, which found that untreated cells exhibited a typical mitotic morphology with condensed chromosomes arranged on the metaphase plate, while oxaliplatin-treated cells underwent little mitosis. However, adavosertib- or combination-treated cells presented loose chromatin, irregularly distributed spindles, micronucleations, and inflated cell shapes, indicating mitotic catastrophe (Fig. 6A and Fig. S11A). In addition, the combination treatment significantly increased the proportion of cells that underwent mitotic catastrophe (Fig. 6B, C). GSEA results further confirmed the activation of apoptosis-related pathways (Fig. S11B, C). Morphologically, cells experiencing mitotic catastrophe exhibited pan-nuclear DNA damage and apoptotic signals, detected by immunofluorescence staining of γ H2AX and cleaved PARP (Fig. 6D and Fig. S11D). Moreover, combined treatment increased apoptosis (Fig. 6E, F) confirmed by increased levels of cleaved PARP and active Caspase-3 in HCC cells (Fig. 6G). Consistent with our *in vitro* findings, the combination treatment synergistically inhibited tumor tissue proliferation and induced greater DNA damage, RS and apoptosis in tumor tissue, as measured by H&E and IHC (Fig. 6H).

In conclusion, oxaliplatin-induced DNA damage activates G2/M checkpoints and blocks the cell cycle before mitosis. Adavosertib, on the other hand, inhibits oxaliplatin-induced activation of HR repair and DNA damage checkpoints, forcing cells with unrepaired damaged DNA into mitosis. This combination causes excessive RS and ultimately induces mitotic catastrophe and apoptosis, producing a significant synergistic effect.

8. The combination of oxaliplatin and adavosertib remains synergistic in hydrodynamic injection models and in sorafenib-resistant cells

In order to investigate whether oxaliplatin and adavosertib work synergistically in cancers with high RS, hydrodynamic injection (HDI) models were constructed and used for two weeks using two oncogenic plasmids capable of activating RS, N-RAS, and C-MYC, and the Sleep Beauty (SB) transposon plasmid^[32, 33] (Fig. 7A). After treating HDI mice with single-agent, combination, or vehicle control for the following two weeks, PET/CT results showed significantly lower

standardized liver uptake values (SUV) in the combination treatment group than the single drug and control groups (Fig. 7B). Moreover, the combination treatment was accompanied by decreases in the number of tumor foci and the liver/body weight ratio (Fig. 7C, D). Survival analysis revealed that mice in the combination groups survived significantly longer than those in the control and single-agent groups (Fig. 7E).

Sorafenib is considered a first-line drug in the treatment of advanced HCC, but clinical resistance remains a problem^[34]. Using a sorafenib-resistant HCC cell model, we investigated the effect of oxaliplatin and adavosertib combined therapy on sorafenib-resistant HCC cell growth. Compared to normal SNU449 cells, our sorafenib-resistant HCC cell line (SNU449-SR) displayed a higher IC₅₀ value (Fig. S12A) and was insensitive to sorafenib (Fig. S12B-D). SNU449-SR cells were inhibited synergistically by adavosertib and oxaliplatin (CI=0.563) in this experiment (Fig. 7F). Moreover, combination therapy significantly reduced colony formation (Fig. 7G) and tumorsphere formation (Fig. 7H and Fig. S12E) efficiencies of SNU449-SR cells compared to each single-agent treatment. As observed in SNU449 cells, results showed that adavosertib inhibits oxaliplatin-activated G2/M checkpoints, leading to a greater accumulation of DNA damage and ultimately synergistically inducing apoptosis in SNU449-SR cells (Fig. 7I-L). These results indicate that oxaliplatin combined with adavosertib still has a strong synergistic effect in high-RS models and sorafenib-resistant models.

9. Potential classification and individualized treatment strategies for patients with HCC based on RS

We re-analyzed the transcriptome data from our cohort and the TCGA cohort to determine if differences exist in RS levels. On the basis of the gene panel response to RS, k-means clustering revealed significantly higher RS scores in tumor tissues. Moreover, 94 patients were divided into two subgroups based on different RS levels (RS-High and RS-Low), which were verified by Gene set variation analysis (GSVA) enrichment scores, and observed that high RS levels were strongly associated with worse prognosis, low histological grade, and high rates of tumor recurrence or metastasis (Fig. 8A, B and Table S14). Interestingly, we also found that WEE1 and CDK1 had higher mRNA expression levels in RS-High patients compared to RS-Low patients (Fig. S13A). These findings were also supported by performing the same analysis using the TCGA cohort (Fig. S13B). In the analysis of imaging data, it has been observed that patients having a lower RS level may experience a better prognosis after undergoing postoperative oxaliplatin treatment as compared

to patients with higher RS levels (Fig. S13C). In addition, no significant difference in immune infiltration levels based on proteomic analysis of immune activation markers was found between RS-High and RS-Low patients (Fig. S13D).

Using a similar approach, clustering subgroups based on HR levels demonstrated significant associations with prognosis, histological grade, and tumor recurrence or metastasis rates (Fig. S14A, B, Table S15). Notably, GSEA scores of RS exhibited a strong correlation with HR scores (Fig. S14C). The clustering subgroups based on RS and HR were significantly correlated as well, with most S-III patients having proliferative features and presenting with an elevated level of RS response and HR activation (Fig. 8C and Table S16). These observations indicate that highly proliferative tumors have increased levels of RS and HR capacity to adapt to the extreme conditions generated by RS. We used patient-derived tumor organoids (PDTO) built in our previous study^[35, 36] and PDX models^[36] to assess whether intrinsic RS levels could be used as potential biomarkers to evaluate the effectiveness of oxaliplatin and avosertib in the treatment of HCC (Fig. 8D). PDTO 1-3 were developed using tissues from patients 1-3, who exhibited high RS levels, whereas, PDTO 4-5 was developed using tissues from patients 4-5 with low RS (Fig. S15A). Treatment of these PDTOs showed that PDTOs from patients with low RS levels were sensitive to oxaliplatin; whereas, those from patients with high RS levels were more sensitive to combination therapy (Fig. 8E, F). In addition, we selected patients 1, 2, 4, and 5 and constructed the PDX 5-8 models. Consistent with the PDTO models, PDX models with low-RS were sensitive to oxaliplatin, whereas high-RS PDX models were less sensitive to oxaliplatin and benefited more from combination therapy (Fig. 8G, H and Fig. S15B, C). These models demonstrated that the combination of oxaliplatin and adavosertib produce strong synergistic tumor suppression, by enhancing DNA damage, RS, and apoptosis (Fig. S15D).

According to the findings above, RS levels may serve as a prognostic indicator for patients with HCC. Patients with higher RS levels may benefit more from the synergistic effect of oxaliplatin and adavosertib, which may have implications for precision medicine (Fig. 8I).

Discussion

The high heterogeneity of HCC makes it one of the deadliest malignancies in the world. Previous therapies designed around a ‘one-size-fits-all’ model have not provided significant clinical benefits for most patients. Numerous existing multi-omics studies have demonstrated that stratifying patients based on characteristics such as genotype and phenotype is not only significant for prognosis but also provides a solid theoretical foundation for clinical medication and personalized treatment^[37-40]. Therefore, individualized treatment for HCC with different genetic profiles is the future of HCC therapy.

With the advancements in omics technology, numerous proteomic and transcriptomic clusters have emerged in HCC. However, due to variations in sample cohorts, geographic locations, depth of omics analysis, typing results, and biological characteristics of subtypes, these clusters possess their own specificities and differences^[4]. Therefore, each study’s multiple types hold unique significance. Previous classification systems, such as those proposed by Hoshida^[41] based on gene expression, introduced an S1-S3 typing scheme, and Boyault^[42] based on HCC genomics technology, proposed a G1-G6 typing scheme, which incorporated clinical and genetic characteristics such as P53, PIK3CA, Wnt/ β -catenin, hepatitis B virus (HBV) copy number, and AFP expression levels. It is worth noting that Gao et al.^[5] performed proteogenomic characterization on 159 patients with HBV-related HCC and identified three subgroups with distinct signaling features and metabolic pathways. The metabolic subgroup had the highest levels of metabolism-related proteins and maintained the best liver function. The proliferation subgroup displayed up-regulated expression of proliferation-associated proteins and had the shortest overall survival. The microenvironmental dysregulation subgroup exhibited down-regulated expression of immunity, inflammatory, and stromal proteins. Although their study focused on HBV-associated HCC and the specific molecular characteristics of each subtype were different from ours, they also suggested a relationship between the proliferative characteristics of liver cancer and prognosis, which supports our conclusions. However, these classifications lack further in-depth studies on the characteristics of high proliferation in HCC and the relationship between replication stress levels.

Importantly, based on this finding, we conducted an in-depth analysis of RS levels in each subtype and found that subtypes with proliferative characteristics had higher levels of RS. We then regrouped the samples according to their RS levels and correlated them with the previous unsupervised clustering results. This approach allowed us to propose a precision medicine treatment

plan targeting specific RS levels, offering both novelty and potential clinical translational significance. Furthermore, after performing unsupervised RS clustering based on clinical samples, we found that RS levels are related to patient prognosis, a conclusion that was replicated in the TCGA database. This enhances the generalizability and significance of our research.

Despite the potential for targeting RS as a therapeutic strategy in managing HCC, research into precise application options remains scarce. To further investigate this, we conducted an analysis of RS levels specifically for the highly proliferative subgroup. Our results revealed that HCC cases from the high proliferation subgroup have higher levels of RS compared to other subgroups, which were also correlated with abnormal cell cycle checkpoints and DNA damage repair mechanisms.

Through preclinical drug screening, we found that oxaliplatin has powerful efficacy in targeting RS to suppress HCC tumor progression. Oxaliplatin is a chemotherapeutic agent that directly targets cell replication. By inhibiting tumor cell proliferation, exogenously inducing DNA damage, and elevating cell RS, it has been shown to improve the survival rates of patients with unresectable HCC. However, some patients are prone to oxaliplatin resistance and tumor recurrence. By combining bioinformatic analysis and unbiased kinome-targeted CRISPR loss-of-function gene screens to identify oxaliplatin-sensitizing targets, we identified WEE1 as a synthetic lethal target with RS in HCC.

As a result of P53 mutations and other defects, most human tumor cells undergo G1/S phase checkpoint inactivation, making them reliant on G2/M checkpoint regulation, which WEE1 plays a crucial role in^[15]. By phosphorylating CDK1 at tyrosine 15, WEE1 induces G2/M phase arrest, providing a sufficient opportunity for DNA repair. The WEE1 inhibitor adavosertib inhibits HR repair, blocks the G2/M checkpoint, and is currently undergoing multiple phase II clinical trials^[28]. However, there have been only a few studies conducted on the use of adavosertib in HCC, especially in combination with other clinically approved drugs. Adavosertib and oxaliplatin exhibited synergistic effects in various *in vitro* and *in vivo* models, including HDI models with high RS properties, which were constructed using mixed RS oncogene plasmids (N-RAS and C-MYC).

Oxaliplatin-induced DNA damage triggers homologous and non-homologous recombination repair and cell cycle checkpoint activation in HCC cells, limiting the accumulation of lethal RS. On the one hand, Adavosertib enhances the effect of oxaliplatin-induced DNA damage, by suppressing oxaliplatin-induced HR repair. Adavosertib, on the other hand, prevents cells with incomplete DNA

repair from entering mitosis at the G2/M checkpoint. Therefore, the combination of adavosertib and oxaliplatin induces lethal DNA damage and an extreme increase in RS, ultimately leading to apoptosis. Further morphological evidence shows that lethal RS caused by the combination leads to extensive chromosomal damage and mitotic catastrophe.

To describe the role of adavosertib in DNA damage repair, we employed a pDR-GFP or pimeJ5-GFP reporter system and observed that adavosertib impaired HR repair but activated NHEJ repair in HCC. Several studies have demonstrated that high-fidelity DDR mechanisms, including DSB repair via HR processes, are defective, resulting in a dependency on compensatory DDR machinery (often error-prone, such as NHEJs)^[43]. However, the findings of this study demonstrate that the compensatory activation of NHEJ upon adavosertib treatment could not alleviate the extensive DNA damage caused by oxaliplatin. Therefore, it is promising to investigate the combined effects of WEE1 inhibition and NHEJ inhibition to comprehensively suppress compensatory DDR activation following oxaliplatin treatment.

Through integrating bioinformatics, intrinsic RS levels were shown to serve as a marker of prognosis and chemotherapy sensitivity in patients with HCC. On one hand, patients with high RS levels had worse prognoses, and there was a large overlap between patients with HCC showing high proliferation characteristics and those showing high RS levels. This may be because tumor cells from these patients have a greater ability to adapt to the extreme genomic stress conditions associated with overactive DNA replication. On the other hand, tumor intrinsic RS levels were found to also serve as a potential biomarker for chemosensitivity. In this study, enhanced RS level was associated with enhanced HR capacity, consistent with recent studies that show enhanced DDR contributions to RS and chemotherapy/radiotherapy tumor resistance. Thus, patients with low RS levels may benefit from oxaliplatin monotherapy, as they tend to be accompanied with milder DDR activation and are more sensitive to oxaliplatin-induced DNA damage and lethal RS accumulation. RS accumulation in tumor cells makes adavosertib and oxaliplatin a more effective combination in patients with high RS levels.

It is significant to further explore whether adavosertib can be effective in oxaliplatin-resistant models. Using an oxaliplatin-resistant HCC cell model, we investigated the effect of combined therapy with oxaliplatin and adavosertib on oxaliplatin-resistant HCC cell growth. Compared to normal SNU449 cells, our oxaliplatin-resistant HCC cell line (SNU449-OR) displayed a higher IC50 value (Fig. S16A) and was insensitive to oxaliplatin (Fig. S16B). G2/M checkpoint-related

proteins, such as WEE1, were significantly upregulated in SNU449-OR cells (Fig. S16C). Additionally, our results show that adavosertib continues to have good efficacy in SNU449-OR cells (Fig. S16D-F). These findings significantly enhance the clinical relevance and application potential of this drug combination.

FOLFOX, a widely used oxaliplatin-based chemotherapy regimen, combines 5-fluorouracil (5-FU), oxaliplatin, and leucovorin^[44]. While 5-FU inhibits thymidylate synthase to block DNA synthesis and oxaliplatin forms crosslinks with DNA to disrupt replication and transcription, these agents do not alter the DNA damage repair capacity, potentially leading to resistance. In contrast, oxaliplatin combined with adavosertib offers mechanistic advantages by inhibiting WEE1 kinase to disrupt DNA repair, thereby enhancing oxaliplatin's efficacy and potentially overcoming resistance. Regarding biosafety, the combination of oxaliplatin and adavosertib reduces gastrointestinal and mucocutaneous reactions compared to FOLFOX, which is associated with broader side effects such as oral ulcers^[45] and hand-foot syndrome^[46, 47]. With current technology, it is challenging to definitively demonstrate which treatment regimen is more effective in clinical settings. However, our preclinical PDO model (Fig. S16G) suggests that adavosertib combined with oxaliplatin is slightly superior to the FOLFOX regimen at the same oxaliplatin concentration. These results indicate that the combination of these two drugs has promising potential for clinical application.

Future research should focus on identifying complementary therapeutic strategies to platinum-based drugs for optimizing cancer treatment outcomes. These comprehensive therapeutic approaches not only significantly enhance the efficacy of platinum-based drugs but also provide patients with safer and more effective treatment options. We recognize that optimizing the pharmacokinetic properties of platinum-based drugs, exploring novel delivery systems, and targeting cancer-specific vulnerabilities are key research directions. First, platinum-based nanoparticles constructed through nanotechnology can significantly improve drug solubility, stability, and bioavailability, enhance drug permeability into tumor tissues, and reduce clearance by the reticuloendothelial system, thereby increasing drug cytotoxicity^[48]. Additionally, designing platinum-based drugs to target the differences in DNA repair mechanisms between cancer cells and normal cells is an important strategy to improve treatment efficacy. This approach enhances selectivity and reduces side effects^[49]. Based on our research, WEE1 inhibitors exhibit strong synthetic lethality with oxaliplatin, and combining these two drugs through nanotechnology for synergistic drug delivery is a feasible strategy for future studies. Future research should further explore these synergistic therapeutic strategies to optimize cancer treatment outcomes, providing patients with safer and more efficient

treatment options.

However, some issues still need to be addressed, one of the most important being diarrhea, a side effect of adavosertib. Due to its hydrophobic nature, adavosertib is currently administered orally, which has low bioavailability and poor pharmacological properties and may cause gastrointestinal side effects. Processing the drug into nanoformulations may optimize the pharmacological properties and bioavailability of adavosertib, reducing the required dosage and minimizing side effects.

In conclusion, our study offers promising insights into precision therapies for HCC at both the proteomic and transcriptomic levels and highlights the potential value of RS in HCC. The results of our study demonstrate that RS levels influence the response to oxaliplatin therapy and that targeting WEE1 signaling can sensitize HCC to this treatment. Additionally, this study demonstrates the potential feasibility of individualized treatment of liver cancer based on RS levels, indicating a need for further clinical research.

Conclusion

Targeted replication stress shows great promise in the treatment of liver cancer based on proteomic and transcriptomic analysis results. WEE1 inhibitor adavosertib and oxaliplatin jointly target replication stress in liver cancer, demonstrating a strong synergistic effect. adavosertib inhibits oxaliplatin induced homologous recombination repair as well as activated cell G2/M checkpoints, leading to extensive chromosomal damage and mitotic catastrophe. The replication stress level in liver cancer patients can be utilized as a biomarker to predict liver cancer prognosis and chemotherapy sensitivity.

Ethics statement

The tissue samples were obtained from patients with HCC who underwent surgery at the First Affiliated Hospital of Zhejiang University School of Medicine. Each patient gave his or her written informed consent. The Ethics Committee of the First Affiliated Hospital of Zhejiang University School of Medicine (Ethics Code 2021-384) approved this study. Animal experiments were approved by the Animal Care Committee of Zhejiang University (Ethics Code 2019-1218)

and conducted in strict compliance with the National Institutes of Health Animal Care and Use Guidelines.

Journal Pre-proofs

Materials and Methods

Sample selection

The specimens were collected from the First Affiliated Hospital of Zhejiang University School of Medicine, Hangzhou, China. This study included all cases with histological evidence of HCC, regardless of their histological grade or surgical stage. Our study excluded patients with advanced stages of the disease, active secondary malignancies, or who had undergone any previous treatment including radiotherapy or chemotherapy in order to ensure the homogeneity of the study population. The clinical data of patients were documented in Table S6, which includes their gender, age, degree of differentiation, TNM stage, smoking status, drinking status, liver cirrhosis, vessel invasion, postoperative radiotherapy and chemotherapy, HBV, HCV, AFP, CA125, and CA19-9 levels, tumor size, tumor numbers, survival status, and recurrence or metastasis status. We obtained data on distant metastases during a follow-up of 80 months. The samples utilized in this study were primary tumors without any associated distance metastases. To de-identify each sample, a new study identification number was assigned, replacing the patient's name or medical record number.

Sample Preparation and Fractionation for DDA Library Generation

The samples were initially homogenized with an MP FastPrep-24 homogenizer. Subsequently, SDT (4% SDS, 100 mM DTT, 100 mM TEAB pH 8.0) was added to the homogenized lysates and further sonicated (this step may be skipped for protein solutions), and boiled for 15 minutes. A BCA Protein Assay Kit (Bio-Rad, USA) was used to quantify the supernatant after spinning the samples at 14000g for 40 minutes. Each sample used in this experiment was combined into one sample to generate a DDA library and conduct quality control testing.

FASP Digestion procedure

FASP was used to digest the proteins. Initially, 100 μ g of proteins were mixed with 30 μ l of SDT buffer (4% SDS, 100 mM DTT, 100 mM TEAB pH 8.0), and detergent was removed with UA buffer (8 M Urea, 100 mM TEAB pH 8.0) by repeated ultrafiltration (Microcon units, 10 kD). After adding 0.05M iodoacetamide to 100 μ l of UA buffer, the samples were incubated in darkness for 30

minutes to block reduced cysteine residues. Filter washing was then carried out thrice utilizing 100 μ l UA buffer followed by washing twice with 100 mM TEAB. Afterwards, the protein suspensions were digested overnight with 2g trypsin (Promega) in a 40 μ l solution of 100mM TEAB buffer at 37 °C, and the peptides were collected as filtrates. A UV spectral density measurement at 280nm was performed to determine the peptide content of the filtrate.

TMTPro labeling

The TMT16-plex reagents (Thermo, A44520) were prepared according to the manufacturer's instructions and diluted fourfold with acetonitrile. For peptide labeling, 20 μ L of TMT reagent was added to each digest at a ratio of 1:5 (sample to tag). Peptides from ten tumor tissue samples were labeled using channel 15 and QC_Mix peptides as internal reference samples were labeled using channel 134N. After checking labeling efficiency, 9 mL of 5% hydroxylamine was added to quench the reaction after pooling and analyzing each sample with MS. The samples were pooled into 27 TMT groups, each with a QC, and desalted with Sep-Pak solid-phase extraction columns of 100 mg. Pooled peptides were fractionated into 20 fractions utilizing Thermo Scientific™ Pierce™ High pH Reversed-Phase Peptide Fractionation Kit. After vacuum centrifugation, each fraction was concentrated and reconstituted in 15 L of 0.1% (v/v) formic acid. Collected peptides were subsequently desalted utilizing C18 Cartridges (Empore™ SPE cartridges C18 (standard density), bed I.D. 7 mm, volume 3 ml, Sigma) and reconstituted in 40 μ l of 0.1% (v/v) formic acid. LC fractionated pooled peptides, and the fractions were combined into 20 fractions before desalting for LC-MS/MS analysis.

Mass Spectrometry Assay

ThermoFisher Scientific's Orbitrap Exploris 480 and EASY-nLC1200 liquid chromatography (LC) pump were used to collect proteomic data. Using a 25 cm column, peptides were separated at 250 nl/min over a 90-minute linear gradient. Using the Orbitrap mass analyzer with a resolution of 60,000 at 200 m/z, 350-1500 m/z was selected for analysis, with a maximum injection time of 40 ms, and a normalized AGC of 300%. To proceed with sequencing, charge states ranging from 2 to 5 were required, and a dynamic exclusion window of 120 s was set. The data were collected in

positive ion mode and centroided online.

Mass spectrometry data analysis

Maxquant was used to analyze MS data, and the Uniprot database was downloaded (<http://www.uniprot.org>). The enzyme was set to trypsin, with the maximum missed cleavage allowed being 1. The carbamidomethylation of cysteine residues (+57.0215 Da) and TMT tags on lysine residues (+229.1629 Da) have been designated as static modifications, while methionine residue oxidation (+15.9949 Da) was set as a variable modification. For protein identification, the reported data were based on a 99% confidence level, with a FDR of 1%.

Cluster analysis of proteins

An analysis of hierarchical clustering was conducted using Cluster 3.0 software (<http://bonsai.hgc.jp/~mdehoon/software/cluster/software.htm>) and Java Treeview software (<http://jtreeview.sourceforge.net>). In addition to the dendrogram, a heat map was provided as a visual representation of the similarity of the observations using the Euclidean distance algorithm and the average linkage clustering algorithm (which uses centroids to cluster observations).

Pathway enrichment analysis

Using DAVID software (<https://david.ncifcrf.gov/>), differentially expressed proteins in tumors, normal adjacent tissue (NAT), and normal adjacent tissues (NAT) were analyzed for Gene Ontology and KEGG pathway enrichment. Based on KEGG pathways and categorical annotations, including the GO term "biological process", Fisher's exact test was used to assess pathway enrichment analysis significance.

Library preparation for RNA-seq, RNA-seq data process, and downstream analysis

RNA was extracted from 10 to 20 mg tissue using the RNeasy Mini Kit (Qiagen, Hilden, Germany).

Agilent 2100 bioanalyzer was used to assess RNA integrity, and NanoDrop 2000 was used to measure RNA concentration (Thermo Fisher Scientific, Wilmington, DE). The full transcriptome sequencing libraries with poly-A enrichment method were prepared using the NEBNext Ultra RNA Directional Library Prep Kit (NEB#420) according to the manufacturer's instructions. The 150 bp paired-end sequencing was performed on a HiSeq X10 sequencer (Illumina, San Diego, CA).

Raw reads were initially processed by Trimmomatic (v0.36) to remove adaptor sequences and bases with low sequencing quality. Trimmed reads were mapped to the GRCh38 reference genome using Hisat2 (v2.1.0). The transcripts were then assembled by Stringtie2 (v2.0.6) with GENCODE v38 annotation data. For the quantification of gene expression, the count matrix was normalized using the Trimmed Means of M values method using edgeR (v3.32.1) R package.

We identified differentially expressed genes between groups using the Wilcox rank-sum test and Bonferroni p-value adjustment. For sample clustering, we chose 5000 genes with the highest median deviation abundance from all genes differentially expressed in tumors, and we then used the non-negative matrix factorization (NMF) method in sequential cluster numbers ranging from two to six, using CancerSubtypes (v1.14.0) R package. The three-cluster result generated by NMF was used for the following analysis based on the silhouette value. The ComplexHeatmap (v2.4.2) R package was used to create the gene-cluster heatmap. The overall survival time difference between patients from three clusters was evaluated by log-rank test using survival (v3.2) R package and visualized by survminer (v0.4.9) R package. When analyzing continuous variables, the ANOVA test was used, whereas categorical variables were analyzed with the Chi-squared test. Based on the differentially expressed genes in each cluster, compared to samples from the remaining two clusters, the GO enrichment and GSEA results were calculated and visualized using clusterProfiler (v3.16.1), msigdb (v7.5.1) and enrichplot (v1.8.1) R package.

Data integrated analysis utilizing TCGA database

In this study, RNA-sequencing data were obtained from The Cancer Genome Atlas (TCGA) and analyzed using the GDCRNATools package. The mRNA expression levels of *CHK1*, *H2AX*, *RAD51*, *DNA-PKCS*, *KU70*, and *CCNE1* mRNA expression in HCC, as well as the overall survival (OS) and disease-free survival (DFS) data, retrieved from the Gene Expression Profiling Interactive Analysis (GEPIA) database (<http://gepia.cancer-pku.cn/>).

Tissue microarray and immunohistochemical staining

According to our previous study^[32, 36, 50], Shanghai Outdo Biotech constructed a 113-tissue microarray cohort specifically for immunohistochemical detection from HCC tumors and normal tissues. IHC was performed by soaking paraffin-embedded tissue sections in xylene paraffin, ethanol rehydrated, and 10% hydrogen peroxide solution for 10 minutes, followed by boiling the repair solution at 100°C for 30 minutes. The sections were then incubated with primary and secondary antibodies at room temperature. Depending on the intensity and area of staining, IHC scores are assigned. Staining intensity score: 0, no staining reaction; 1, mild reaction; 2, moderate reaction; 3, strong reaction. Staining area score: 0 (0%), 1 (30%), 2 (30-60%), and 3 (>60%). Multiplying intensity and area scores resulted in the final score. The final WEE1 scores of all HCC tumor tissues were divided into two groups: WEE1-Low (< 4) and WEE1-High (≥4).

Animal experiments

This study used mice obtained from the Shanghai Experimental Animal Center of the Chinese Academy of Sciences (C57BL/6, NOD-SCID or nude, 4-6 weeks old).

Based on our previous study^[36] we established PDX models using human HCC tumor tissues obtained from patients undergoing surgical resection at The First Affiliated Hospital, Zhejiang University School of Medicine. The tumor size was 100 to 200 mm³ three weeks after xenograft inoculation, and all mice were randomly divided into eight groups (Vehicle; gemcitabine, 100 mg/kg, i.v., twice a week; sorafenib, 60 mg/kg, p.o., Q.d.; oxaliplatin, 10 mg/kg, i.p., Qw; epirubicin HCl, 3.5 mg/kg, i.v., Q.d.; 5-FU, 50mg/kg, i.p., twice a week; irinotecan, 15 mg/kg, i.p., Once every five days; paclitaxel, 10 mg/kg, i.v., twice a week).

We established subcutaneous and orthotopic xenograft models using HCC cells in mice^[50]. For the subcutaneous xenograft model, we injected HCC cells subcutaneously (4×10^6 cells/100 μ L PBS) and initiated treatments when tumors reached 100-200 mm³ after random grouping. For the orthotopic xenograft model, we employed small live animal imaging techniques using D-luciferase sodium salt (Yeasen, Shanghai, China). Hepa1-6 cells were transfected with luciferase and injected into the liver's right lobe of C57BL/6 mice. After two weeks of tumor growth, mice underwent drug treatment for another two weeks before analysis. We followed guidelines for animal handling and

care throughout the experiment.

The drug regimen included four groups: vehicle, oxaliplatin (10 mg/kg every 3 days, intravenously), adavosertib (50 mg/kg once daily, intravenously), and a combination of both treatments. We initiated treatments when tumors reached 100-200 mm³ after random grouping into four groups: vehicle, oxaliplatin, adavosertib, and the combination of oxaliplatin and adavosertib, and continued for two weeks. At the end of treatment, tumors were harvested and analyzed using assays, as well as tumor size measurements every other day.

Cell culture

Human HCC cell lines (SNU449, PLC/PRF/5, HepG2, Hep3B, SNU182, SNU387, HCCLM3, Huh6, Huh7, SK-Hep-1) and mouse HCC cell line (Hepa 1-6) were purchased from the Shanghai Cell Bank, Chinese Academy of Sciences, and were cultured in recommended medium supplemented with 10% fetal bovine serum (FBS) and 1% penicillin/streptomycin. CCTCC performed short tandem repeat sequence (STR) profiling on all cell lines to prevent cross-contamination. Every 15 passages, the cells are expanded and frozen, and mycoplasma contamination is confirmed negative for all cell lines.

Synthetic lethal screens

From Vigenebio, we procured the human kinome gRNA library lentivirus, which contains 3,052 unique sequence-guided RNAs targeting 763 human kinase genes. Lentiviral transduction was used to introduce the kinome CRISPR library into HCC cells. lentiGuide-Puro (lentivirus containing a pooled kinome-scale CRISPR knockout library) was transfected into Huh7 cells and cultured with oxaliplatin or without it. Genomic DNA was isolated after two weeks of incubation, and guide RNA abundance was determined by high-throughput sequencing before MAGeCKFlute analysis. An Illumina deep sequencing analysis was performed on pooled samples of stably expressing sgRNA cells cultured for 14 days. By using MAGeCK's mle module, raw sgRNA counts were uploaded into the algorithm to determine gene significance (beta scores) using maximum likelihood estimates. Oxaliplatin synthetic lethal genes were identified by filtering for a beta score > 1 and $p < 0.05$ in the treatment group but a beta score ≤ 1 in the control group.

Cell viability, colony formation, and oncosphere formation assays.

As previously described^[32], viability and colony formation assays were performed. Briefly, HCC cells were inoculated overnight and exposed to the indicated doses of oxaliplatin and adavorsertib combination for 2 days. The viability of the cells was determined using the Cell Counting Kit-8 (Dojindo Molecular Technologies, Rockville, MD, USA). Each dose of the drug combination was tested in six replicates. Chou-Talalay calculated the combination index (CI) as a measure of drug synergy^[51].

For the oncosphere formation assay, we prepared cells in a serum-free medium, seeded them in ultra-low attachment plates (Corning, USA), and allowed them to grow for six hours. The 3D oncospheres of cells were photographed after 5-7 days with a fluorescence microscope (OLYMPUS, IX81).

During the colony formation assay, cells were incubated overnight. Following 10 days of treatment, various doses of drug combinations were used. The cells were stained with Jimsa (Nanjing, Jiancheng Technology). Each well of the plate was then photographed and analyzed.

Cell migration and invasion assay

To perform cell migration and invasion experiments, serum-free medium 300 μ L containing 2×10^4 HCC cells in different treatment groups was added to Transwell culture chamber pre-treated with or without Matrigel (BD Biosciences, San Jose, CA, USA). 700 μ L medium containing 10% FBS was added to the lower chamber. The cells that migrated or invaded outside the filters were then stained and photographed for analysis.

Wound healing assay

To allow cells to adhere to the wells, cells from different treatment groups were inoculated into wells and cultured for 24 hours. A cell-free gap was then created by removing the culture insert. Cells were cultured in a serum-free medium for drug treatments, photographed and the distance on

either side of the cell border was measured at different time points.

RNA sequencing and data processing

The Huh7 cells were inoculated into 10 cm diameter culture dishes and treated with various drugs for 24 hours. Cells were collected in RIPA buffer for RNA sequencing. RNA sequencing services were provided by Genedenovo Co.(Guangzhou, China), using Illumina HiSeq 2500 (Illumina, USA). Differential expression analysis was performed using DEseq2 (v3.14.0) in the R statistical environment (v3.5).

Western blot analysis

We prepared protein extracts on ice with RIPA cell lysis buffers (Thermo Scientific, Waltham, MA, USA) containing phosphatase inhibitors (1:100). Western blot analysis was performed on lysates and prestained protein markers (M221, GenStar, Beijing, China) after SDS-PAGE and PVDF membrane transfer. TBST (Tris-buffered saline and 0.1% Tween-20) with 5% nonfat dry milk was used for blocking the membranes for one hour, before primary and secondary antibodies (Table S17) were incubated and analyzed by Bio-Rad.

Immunofluorescence assay

After seeding HCC cells into confocal dishes (20,000 cells per dish) overnight, cells were washed with PBS and fixed with 4% paraformaldehyde for 10 minutes. Incubation was performed overnight with primary antibodies diluted with antibody dilution buffer (1% BSA and 0.5% TritonX-100 in PBS) after permeabilization and blocking with 4% bovine serum albumin (BSA) (Absin, Shanghai, China). The cells were incubated with the appropriate secondary antibody (EarthOx, USA) for 1 hour in the dark. In the final step, cells were stained with DAPI (Sigma-Aldrich, USA) for 10 minutes and imaged using a high-resolution confocal microscope (Olympus, Japan).

Comet assay

Perform comet assays using CometAssay Kit (Trevigen) and the mean tail moment was calculated as an index of DNA damage by using CASP software.

Analysis of DSB repair by HR reporter assays and NHEJ reporter assays

As previously stated, the effectiveness of DNA double-strand break repair was assessed utilizing GFP-based reporter gene experiments. Cells were cotransfected with pDRGFP or pimEJ5-GFP and I-Sce1 expression plasmids to induce DSBs. Flow cytometry was used to determine HR and NHEJ efficiency 24 hours after treatment.

Cell cycle and apoptosis analysis

After synchronization in no-serum medium for 48 hours, the HCC cells were released and cultured in complete medium for further cell cycle analysis. After fixing the cells in 75% ethanol overnight at 4 °C, the cells were stained with DNA Prep (Beckman Coulter, Brea, CA, USA), and flow cytometry was used to analyze the proportion of cells in each phase of the cell cycle.

Following the manufacturer's instructions, we collected, washed, and stained HCC cells with FITC-conjugated Annexin V and propidium iodide to analyze apoptosis. The percentage of apoptotic cells was analyzed using flow cytometry. GFP-positive cells.

Metaphase spread assays

At 37°C, cells were exposed to Colchicine (100 ng/ml) (#HY-16569, MedChemExpress) for 2 to 3.5 hours and 75 mM KCl for 30 minutes. After fixation in methanol:acetic acid (3:1) at 4°C overnight, the slides were air-dried, stained with DAPI, and coded for blind analysis.

Hydrodynamic injection models

We performed the HDI model on C57BL/6 mice by injecting PBS containing 10 μ g of Sleeping Beauty (SB) transposon, 15 μ g of C-MYC, and 15 μ g of N-RAS plasmid through the tail vein within 5-7 seconds, as described in our previous study^[32,33,50]. After two weeks of injection, the mice were treated with drugs for another two weeks. They were sacrificed and the liver weights were determined. The growth of primary liver tumor foci in mice was observed using micro PET/CT. The survival time of mice was recorded for overall survival analysis.

Patient-derived tumor organs (PDTOs) screening drug models

PDTO models were constructed as described in our previous study^[35]. Following cure of the hydrogels, successful PDTOs were cultured for five days, followed by seven days of drug administration. PDTO live/dead cell staining was performed using a Calcein-AM/PI double staining kit (Dojindo). Confocal microscopy was used for quantitative analysis of the staining.

Bioinformatics analysis

Replication stress genes (R-HSA-176187) and homologous recombination repair genes (R-HSA-5693579) were obtained from MSigDB. The single-sample gene set enrichment analysis (ssGSEA) score was calculated using the GSVA R package with default parameters based on replication stress or homologous recombination repair genes. K-means clustering was performed using ConsensusClusterPlus R package based on 37 replication stress-related genes or homologous recombination repair-related genes. The default parameters of CIBERSORT were used to analyze the tumor infiltrating immune cell profile, with significant p-values derived from limma R package.

Statistical analysis

GraphPad Prism and SPSS 19.0 for Windows programs and Prism GraphPad (GraphPad Software Inc, San Diego, CA, USA) were used for all statistical analyses. The data were expressed as mean \pm standard deviation (SD). Kaplan-Meier survival analysis and log-rank tests were used for the overall survival analysis. Students' two-tailed t-tests or one-way analysis of variance (ANOVA) were used to measure differences between groups. P-values are indicated by * for $P < 0.05$, ** for

$P < 0.01$, and *** for $P < 0.001$.

Data availability

Upon reasonable request, the corresponding authors can provide data supporting this study's findings.

Ethics statement

The tissue samples were obtained from patients with HCC who underwent surgery at the First Affiliated Hospital of Zhejiang University School of Medicine. Each patient gave his or her written informed consent. The Ethics Committee of the First Affiliated Hospital of Zhejiang University School of Medicine (Ethics Code 2021-384) approved this study. Animal experiments were approved by the Animal Care Committee of Zhejiang University (Ethics Code 2019-1218) and conducted in strict compliance with the National Institutes of Health Animal Care and Use Guidelines.

References:

- [1] Sung H, Ferlay J, Siegel RL, et al. Global cancer statistics 2020: Globocan estimates of incidence and mortality worldwide for 36 cancers in 185 countries. *CA Cancer J Clin*, 2021, 71: 209-249
- [2] Easl clinical practice guidelines: Management of hepatocellular carcinoma. *J Hepatol*, 2018, 69: 182-236
- [3] Zucman-Rossi J, Villanueva A, Nault J-C, et al. Genetic landscape and biomarkers of hepatocellular carcinoma. *Gastroenterology*, 2015, 149:
- [4] Wu Y, Liu Z, Xu X. Molecular subtyping of hepatocellular carcinoma: A step toward precision medicine. *Cancer Commun (Lond)*, 2020, 40: 681-693
- [5] Gao Q, Zhu H, Dong L, et al. Integrated proteogenomic characterization of hbv-related hepatocellular carcinoma. *Cell*, 2019, 179: 1240
- [6] Saxena S, Zou L. Hallmarks of DNA replication stress. *Mol Cell*, 2022, 82: 2298-2314
- [7] Gaillard H, García-Muse T, Aguilera A. Replication stress and cancer. *Nat Rev Cancer*, 2015, 15: 276-289
- [8] da Costa AABA, Chowdhury D, Shapiro GI, et al. Targeting replication stress in cancer therapy. *Nat Rev Drug Discov*, 2023, 22: 38-58
- [9] Cybulla E, Vindigni A. Leveraging the replication stress response to optimize cancer therapy. *Nat Rev Cancer*, 2023, 23:
- [10] Li Q-J, He M-K, Chen H-W, et al. Hepatic arterial infusion of oxaliplatin, fluorouracil, and leucovorin versus transarterial chemoembolization for large hepatocellular carcinoma: A randomized phase iii trial. *J Clin Oncol*, 2022, 40: 150-160
- [11] Qin S, Bai Y, Lim HY, et al. Randomized, multicenter, open-label study of oxaliplatin plus fluorouracil/leucovorin versus doxorubicin as palliative chemotherapy in patients with advanced hepatocellular carcinoma from asia. *J Clin Oncol*, 2013, 31: 3501-3508

- [12] Ma L, Xu A, Kang L, et al. Lsd1-demethylated linc01134 confers oxaliplatin resistance through sp1-induced p62 transcription in hcc. *Hepatology*, 2021, 74: 3213-3234
- [13] Liu S, Bu X, Kan A, et al. Sp1-induced lncrna dubr promotes stemness and oxaliplatin resistance of hepatocellular carcinoma via e2f1-cip2a feedback. *Cancer Lett*, 2022, 528: 16-30
- [14] Sun F, Liu Y, Gong T, et al. Inhibition of dtymk significantly restrains the growth of hcc and increases sensitivity to oxaliplatin. *Cell Death Dis*, 2021, 12: 1093
- [15] Ghelli Luserna di Rorà A, Cerchione C, Martinelli G, et al. A wee1 family business: Regulation of mitosis, cancer progression, and therapeutic target. *Journal of Hematology & Oncology*, 2020, 13: 126
- [16] Elbæk CR, Petrosius V, Benada J, et al. Wee1 kinase protects the stability of stalled DNA replication forks by limiting cdk2 activity. *Cell Rep*, 2022, 38: 110261
- [17] Murga M, Campaner S, Lopez-Contreras AJ, et al. Exploiting oncogene-induced replicative stress for the selective killing of myc-driven tumors. *Nat Struct Mol Biol*, 2011, 18: 1331-1335
- [18] Dreyer SB, Upstill-Goddard R, Paulus-Hock V, et al. Targeting DNA damage response and replication stress in pancreatic cancer. *Gastroenterology*, 2021, 160:
- [19] Pan T, Qin Q, Nong C, et al. Author correction: A novel wee1 pathway for replication stress responses. *Nat Plants*, 2021, 7: 376
- [20] Liu JF, Xiong N, Campos SM, et al. Phase ii study of the wee1 inhibitor adavosertib in recurrent uterine serous carcinoma. *J Clin Oncol*, 2021, 39: 1531-1539
- [21] Moore KN, Chambers SK, Hamilton EP, et al. Adavosertib with chemotherapy in patients with primary platinum-resistant ovarian, fallopian tube, or peritoneal cancer: An open-label, four-arm, phase ii study. *Clinical Cancer Research : an Official Journal of the American Association For Cancer Research*, 2022, 28: 36-44
- [22] Lheureux S, Cristea MC, Bruce JP, et al. Adavosertib plus gemcitabine for platinum-resistant or platinum-refractory recurrent ovarian cancer: A double-blind, randomised, placebo-controlled, phase 2 trial. *Lancet*, 2021, 397: 281-292

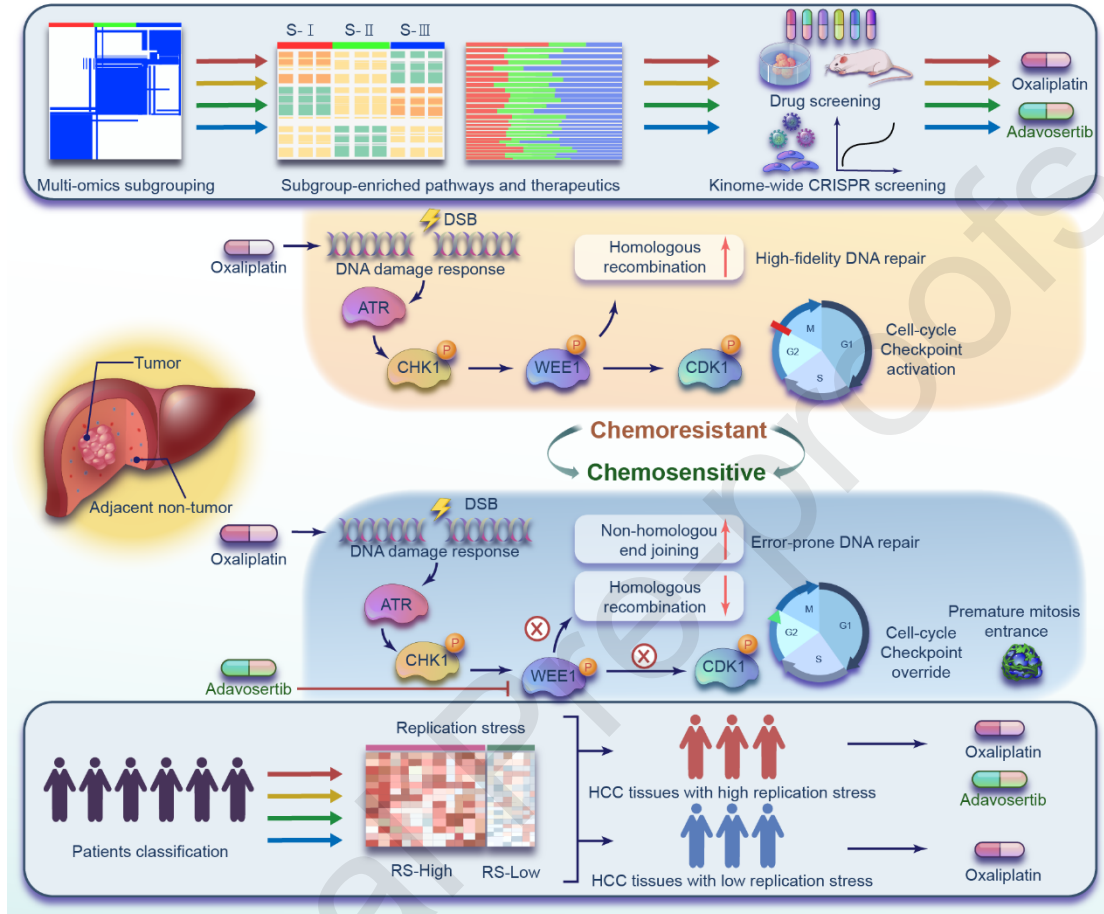
- [23] Keenan TE, Li T, Vallius T, et al. Clinical efficacy and molecular response correlates of the wee1 inhibitor adavosertib combined with cisplatin in patients with metastatic triple-negative breast cancer. *Clinical Cancer Research : an Official Journal of the American Association For Cancer Research*, 2021, 27: 983-991
- [24] Huang A, Yang X-R, Chung W-Y, et al. Targeted therapy for hepatocellular carcinoma. *Signal Transduct Target Ther*, 2020, 5: 146
- [25] He M, Li Q, Zou R, et al. Sorafenib plus hepatic arterial infusion of oxaliplatin, fluorouracil, and leucovorin vs sorafenib alone for hepatocellular carcinoma with portal vein invasion: A randomized clinical trial. *JAMA Oncol*, 2019, 5: 953-960
- [26] Kannaiyan R, Mahadevan D. A comprehensive review of protein kinase inhibitors for cancer therapy. *Expert Rev Anticancer Ther*, 2018, 18: 1249-1270
- [27] Doench JG, Fusi N, Sullender M, et al. Optimized sgrna design to maximize activity and minimize off-target effects of crispr-cas9. *Nat Biotechnol*, 2016, 34: 184-191
- [28] Fu S, Yao S, Yuan Y, et al. Multicenter phase ii trial of the wee1 inhibitor adavosertib in refractory solid tumors harboring ccne1 amplification. *J Clin Oncol*, 2023, 41: 1725-1734
- [29] Bukhari AB, Lewis CW, Pearce JJ, et al. Inhibiting wee1 and atr kinases produces tumor-selective synthetic lethality and suppresses metastasis. *J Clin Invest*, 2019, 129: 1329-1344
- [30] Li S, Wang L, Wang Y, et al. The synthetic lethality of targeting cell cycle checkpoints and parps in cancer treatment. *Journal of Hematology & Oncology*, 2022, 15: 147
- [31] Ubhi T, Brown GW. Exploiting DNA replication stress for cancer treatment. *Cancer Research*, 2019, 79: 1730-1739
- [32] Zhu X, Song G, Zhang S, et al. Asialoglycoprotein receptor 1 functions as a tumor suppressor in liver cancer via inhibition of stat3. *Cancer Research*, 2022, 82: 3987-4000
- [33] Chen J, Xuan Z, Song W, et al. Eag1 enhances hepatocellular carcinoma proliferation by modulating skp2 and metastasis through pseudopod formation. *Oncogene*, 2021, 40: 163-176

- [34] Lyu N, Wang X, Li J-B, et al. Arterial chemotherapy of oxaliplatin plus fluorouracil versus sorafenib in advanced hepatocellular carcinoma: A biomolecular exploratory, randomized, phase iii trial (fohaic-1). *J Clin Oncol*, 2022, 40: 468-480
- [35] Dong H, Li Z, Bian S, et al. Culture of patient-derived multicellular clusters in suspended hydrogel capsules for pre-clinical personalized drug screening. *Bioact Mater*, 2022, 18: 164-177
- [36] Zhang S, Jia X, Dai H, et al. Serpine2 promotes liver cancer metastasis by inhibiting c-cbl-mediated egfr ubiquitination and degradation. *Cancer Commun (Lond)*, 2024, 44: 384-407
- [37] Diao P, Dai Y, Wang A, et al. Integrative multiomics analyses identify molecular subtypes of head and neck squamous cell carcinoma with distinct therapeutic vulnerabilities. *Cancer Research*, 2024, 84: 3101-3117
- [38] Gong Y, Ji P, Yang Y-S, et al. Metabolic-pathway-based subtyping of triple-negative breast cancer reveals potential therapeutic targets. *Cell Metab*, 2021, 33:
- [39] Migliozzi S, Oh YT, Hasanain M, et al. Integrative multi-omics networks identify pkc δ and DNA-pk as master kinases of glioblastoma subtypes and guide targeted cancer therapy. *Nat Cancer*, 2023, 4: 181-202
- [40] Liu Y, Xun Z, Ma K, et al. Identification of a tumour immune barrier in the hcc microenvironment that determines the efficacy of immunotherapy. *J Hepatol*, 2023, 78: 770-782
- [41] Hoshida Y, Nijman SMB, Kobayashi M, et al. Integrative transcriptome analysis reveals common molecular subclasses of human hepatocellular carcinoma. *Cancer Research*, 2009, 69: 7385-7392
- [42] Boyault S, Rickman DS, de Reyniès A, et al. Transcriptome classification of hcc is related to gene alterations and to new therapeutic targets. *Hepatology*, 2007, 45: 42-52
- [43] Atkinson J, Bezak E, Le H, et al. DNA double strand break and response fluorescent assays: Choices and interpretation. *Int J Mol Sci*, 2024, 25:
- [44] Mastrantoni L, Chiaravalli M, Spring A, et al. Comparison of first-line chemotherapy regimens in unresectable locally advanced or metastatic pancreatic cancer: A systematic review and bayesian network meta-analysis. *Lancet Oncol*, 2024, 25: 1655-1665

- [45] Mohammed AI, Celentano A, Paolini R, et al. Characterization of a novel dual murine model of chemotherapy-induced oral and intestinal mucositis. *Sci Rep*, 2023, 13: 1396
- [46] Chiara S, Nobile MT, Barzacchi C, et al. Hand-foot syndrome induced by high-dose, short-term, continuous 5-fluorouracil infusion. *Eur J Cancer*, 1997, 33: 967-969
- [47] Yen-Revollo JL, Goldberg RM, McLeod HL. Can inhibiting dihydropyrimidine dehydrogenase limit hand-foot syndrome caused by fluoropyrimidines? *Clinical Cancer Research : an Official Journal of the American Association For Cancer Research*, 2008, 14:
- [48] Yu B, Wang Y, Bing T, et al. Platinum prodrug nanoparticles with cox-2 inhibition amplify pyroptosis for enhanced chemotherapy and immune activation of pancreatic cancer. *Adv Mater*, 2024, 36: e2310456
- [49] Kiss RC, Xia F, Acklin S. Targeting DNA damage response and repair to enhance therapeutic index in cisplatin-based cancer treatment. *Int J Mol Sci*, 2021, 22:
- [50] Chen J, Li Z, Jia X, et al. Targeting anillin inhibits tumorigenesis and tumor growth in hepatocellular carcinoma via impairing cytokinesis fidelity. *Oncogene*, 2022, 41: 3118-3130
- [51] Chou T-C. Drug combination studies and their synergy quantification using the chou-talalay method. *Cancer Research*, 2010, 70: 440-446

Figure legends

Graphical Abstract



A schematic model of the mechanism by which WEE1 kinase inhibitor AZD1775 improves chemotherapy sensitivity in HCC patients, as well as a potential precision drug treatment strategy for HCC patients.

Figure 1

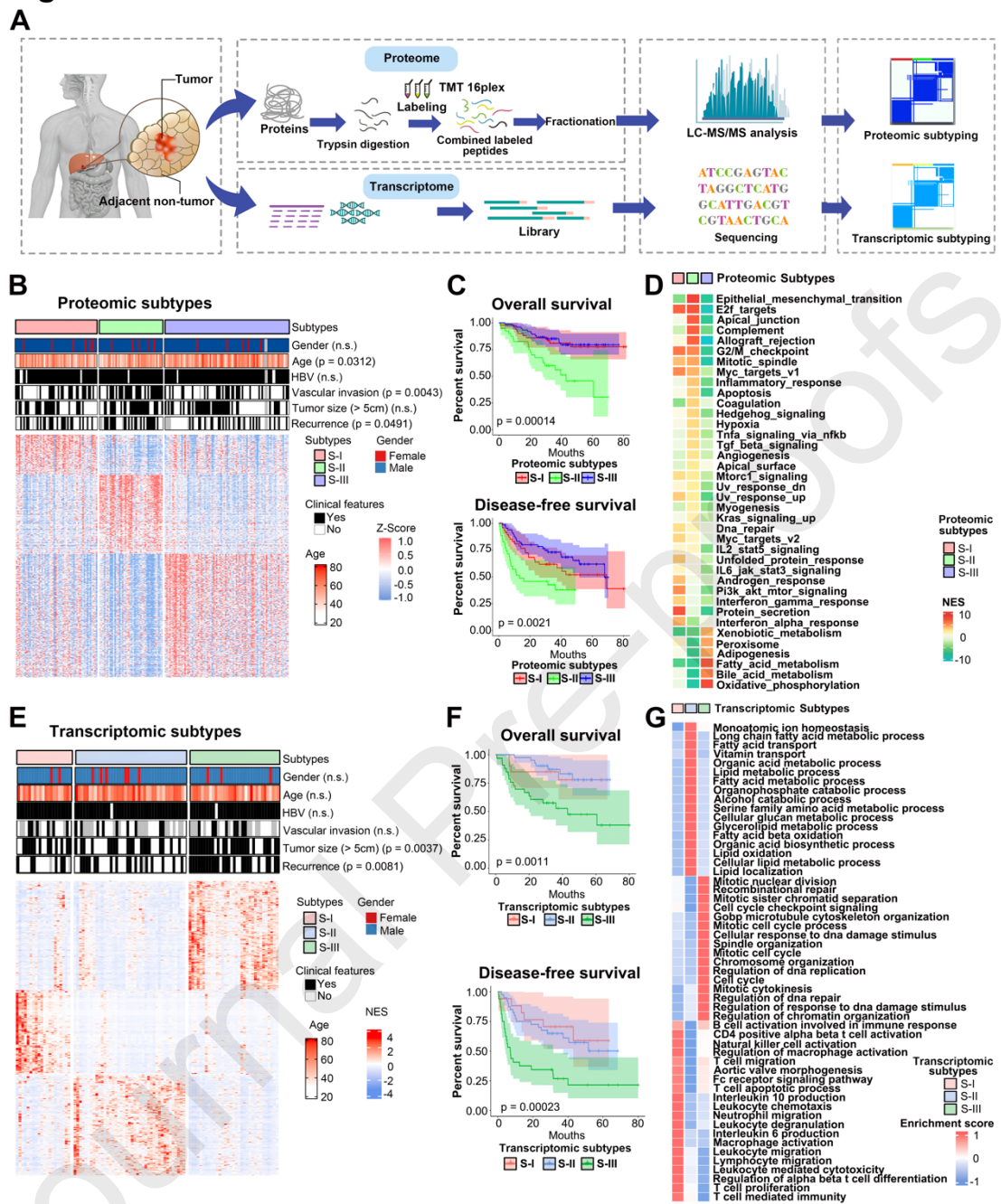


Figure 1. Molecular subtypes of HCC identified using proteomic and transcriptomic analyses.

(A) The experimental design and the number of samples used for proteomic and transcriptomic analyses were summarized. (B) Subtyping results based on the 178 HCC tumor enrichment scores in the HCC proteomic samples; S-I (red, n = 54), S-II (green, n = 42), and S-III (blue, n = 82). The heat map shows the Z-Score of the three subtypes. Grey represents the absence of patient clinical information. (C) Kaplan–Meier curves of overall survival (OS) and disease-free survival (DFS) among the 3 proteomic subtypes in the HCC cohort. Log-rank test and BH method for adjusting P

value. Among all proteomic subtypes, $P = 0.00014$ (OS); $P = 0.0021$ (DFS). (D) Integrated analysis of differentially activated metabolic and signaling pathways among the three proteomic subtypes. (E) Subtyping results based on the 94 HCC tumor enrichment scores in the HCC transcriptomic samples; S-I (red, $n = 20$), S-II (blue, $n = 33$), and S-III (green, $n = 41$). The heat map shows normalized enrichment scores (NES) of the 3 subtypes. Grey represents the absence of patient clinical information. (F) Kaplan–Meier curves of OS and DFS among the 3 transcriptomic subtypes in the HCC cohort. Log-rank test and BH method for adjusting P value. Among all transcriptomic subtypes, $P = 0.0011$ (OS); $P = 0.00023$ (DFS). (G) Integrated analysis of differentially activated metabolic and signaling pathways among the three transcriptomic subtypes.

Figure 2

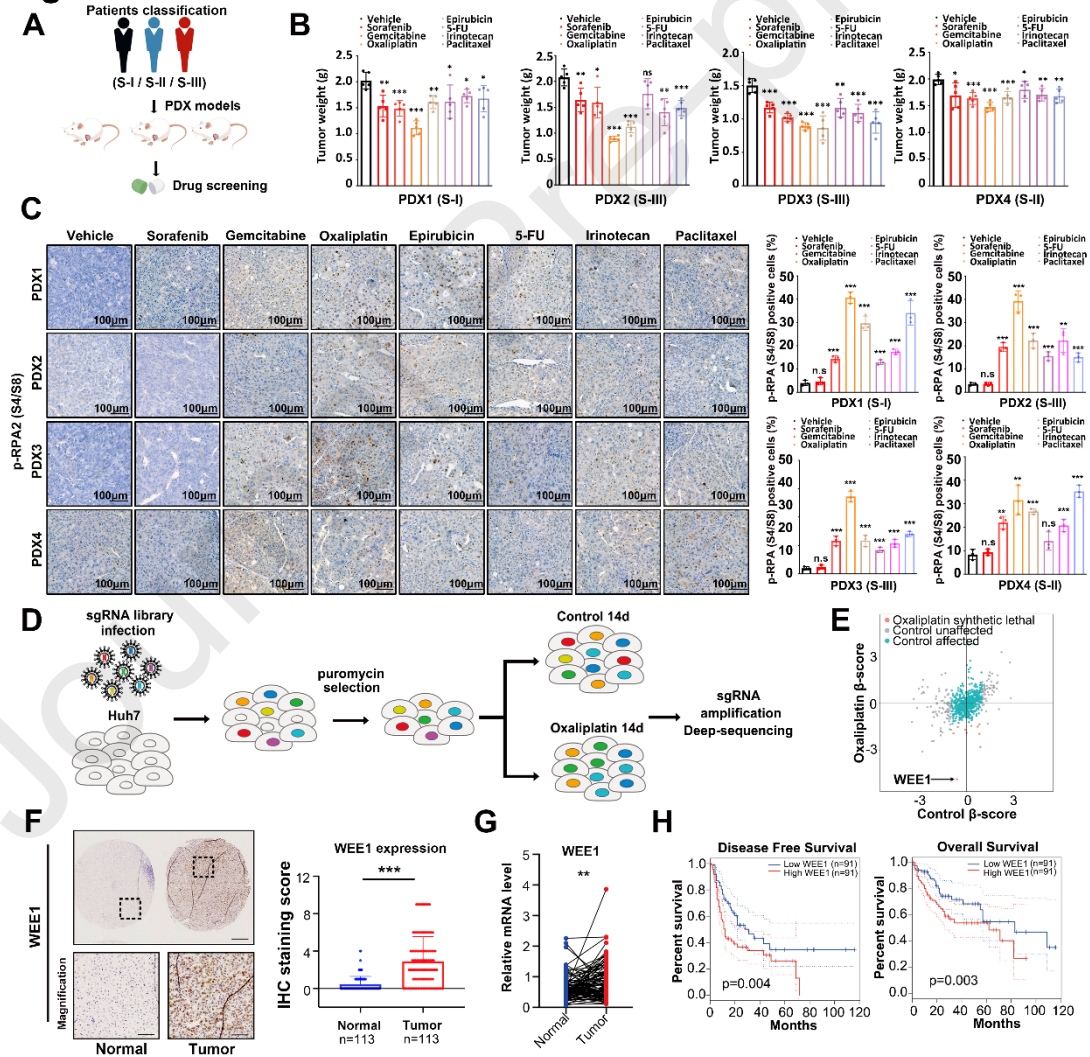


Figure 2. WEE1 was identified as a synthetic lethal gene targeted by oxaliplatin, promoting

replication stress accumulation in HCC.

(A) Schematic of construction of PDX models of different proteomic subtypes. (B) The HCC xenografts of PDX models were measured every three days after inoculation. Tumor weight (g) of HCC xenografts in PDX 1 to PDX 4 from the different groups were shown (n = 5 per group). (C) IHC staining results of p-RPA2 (S4/S8) and the quantification of the indicated treatment groups from the PDX models. Scale bars, 100 μ m. (H) Schematic of the CRISPR-Cas9 library screen. (D, E) Scatter plot of beta-score in control and oxaliplatin-treated group. Red dots represent genes decreased only in the oxaliplatin-treated group (n = 10). WEE1 was found to be most significantly altered according to differential beta-score and was labeled. (F) Representative TMA stained images illustrating WEE1 expression levels in tumors and adjacent non-tumor tissues from HCC patients (left panel). This cohort is an additional, specifically designed group for IHC staining on tissue microarrays. IHC scores quantifying WEE1 expression in matched tumor and non-tumor tissues from 113 liver cancer patients are presented on the right panel. (G) Relative mRNA expression levels of CDK1, and WEE1 in HCC tumor (T) versus normal (N) tissues (n = 94). (H) The disease-free survival and overall survival analysis of patients with LIHC in WEE1 high-level and low-level groups from the TCGA and GTEx databases by GEPIA. Data are shown as mean \pm SD. ***P < 0.001; **P < 0.01; *P < 0.05; n.s., not significant.

Figure 3

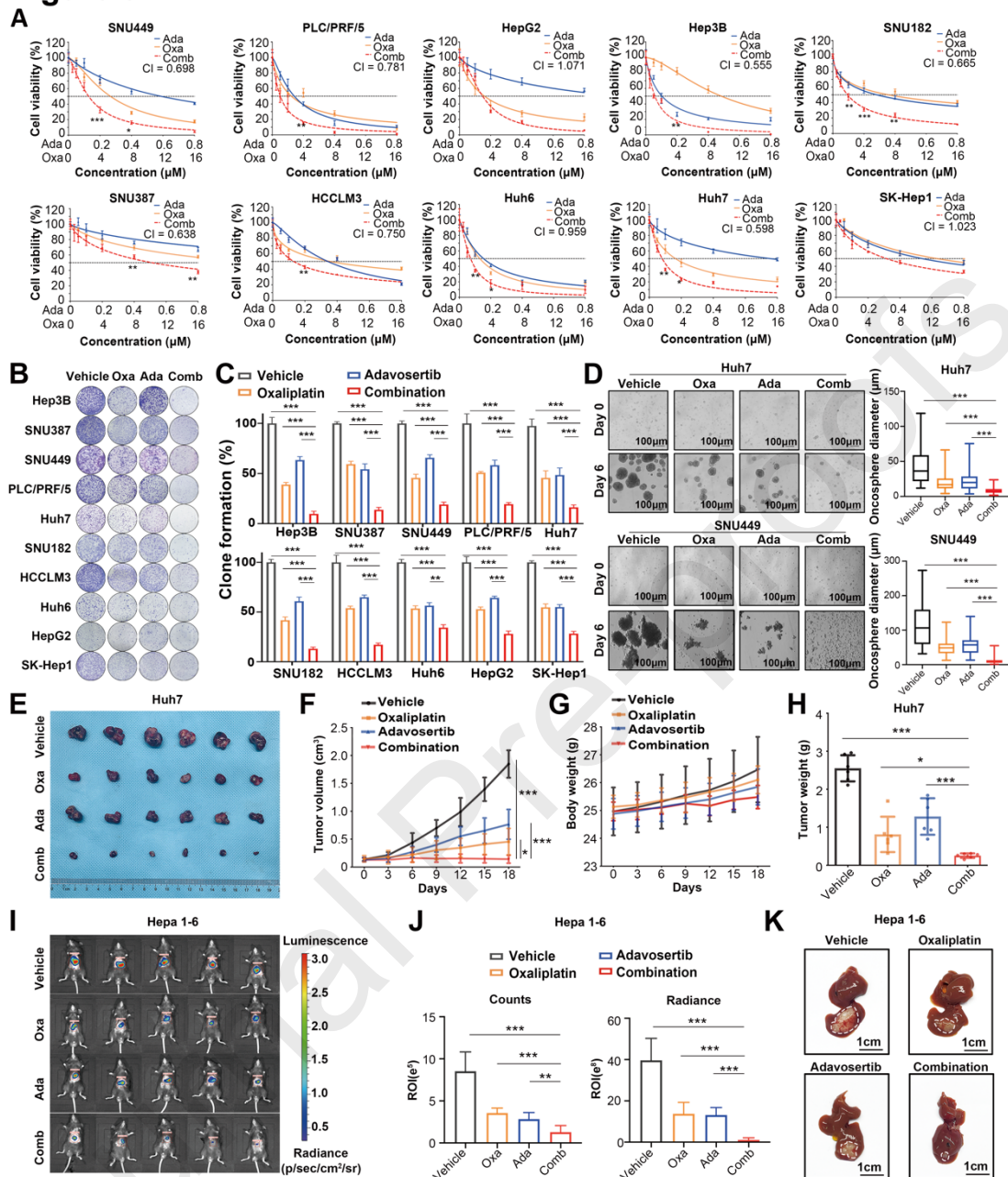


Figure 3. Inhibition of WEE1 by adavosertib induces synergistic cytotoxic effects with oxaliplatin in vitro and in vivo.

A) Dose-response curve of the indicated human HCC cell lines treated with adavosertib (blue), oxaliplatin (orange), and adavosertib + oxaliplatin (red), from a 2-day CCK-8 assay ($n = 6$ per group). Drug synergies of each cell line were determined by the combination index (CI) calculated by the Chou-Talalay method. The combination index (CI) quantitatively depicts synergism ($CI < 1$). (B, C) Colony formation assays of HCC cells exposed to oxaliplatin (2 μ M) and/or Adavosertib

(100 nM). Colonies containing more than 50 cells were counted after 10-14 days of treatment (n = 3 per group). (D) Oncosphere formation assays were performed on Huh7 and SNU449 cells cultured with oxaliplatin (10 μ M) and/or adavosertib (500 nM) grown for 7 days (n = 3 per group). The scale bar is 2 μ m. (E-H) Tumor volume (mm^3), tumor weight (g), and the body weight of the Huh7 xenograft models were assessed in different treatment groups (n = 6 per group). (I) The images of small living animal imaging using D-luciferin sodium salt were shown (n = 5 per group). (J) Radiance and counts of different treatment groups were shown (n = 5 per group). (K) Representative images indicated tumors with white circles (n = 5 per group). Scale bars, 1 cm. Data are shown as mean \pm SD. ***P < 0.001; **P < 0.01; *P < 0.05; n.s., not significant.

Figure 4

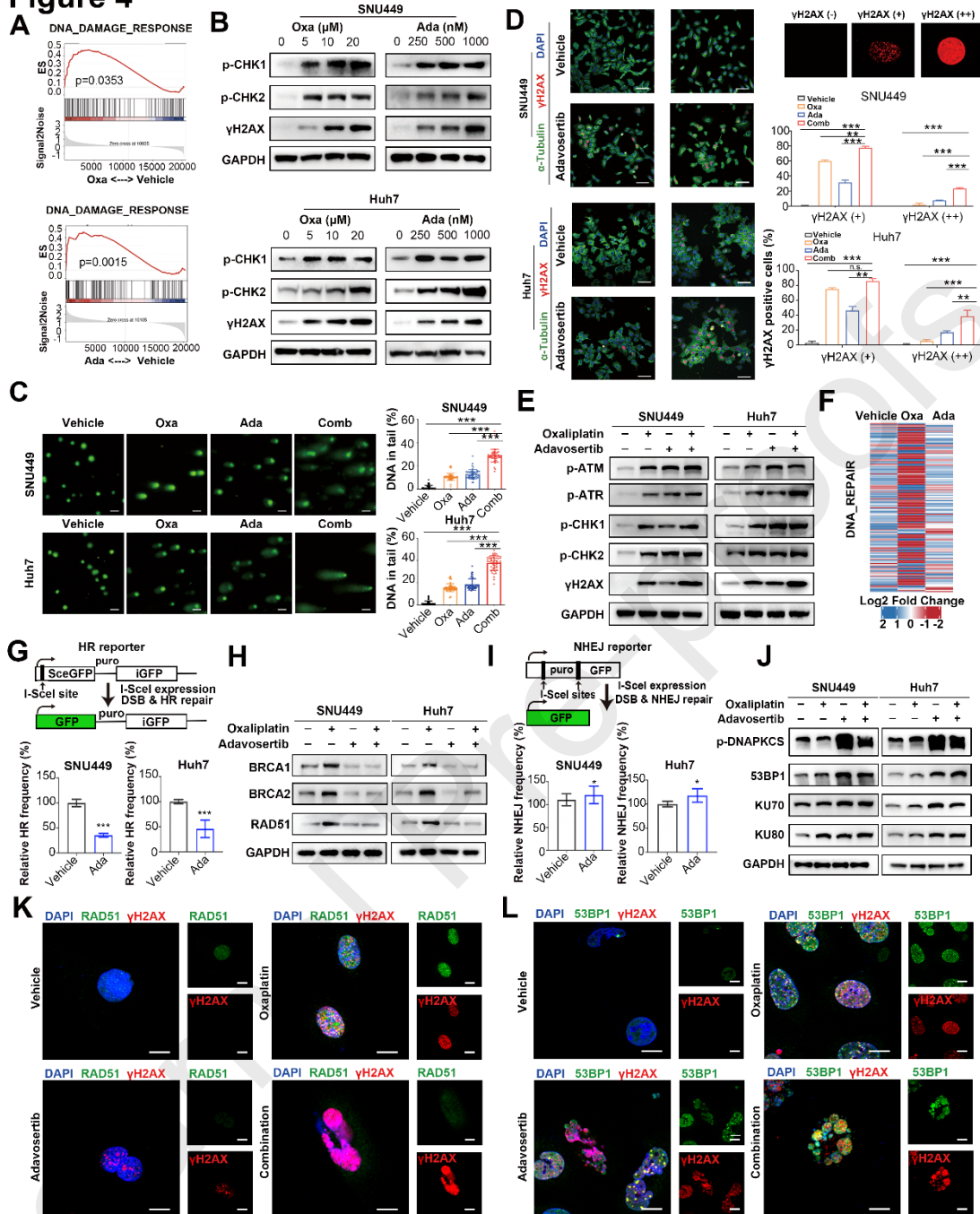


Figure 4. Synergistic enhancement of oxaliplatin-induced DNA damage by adavosertib through homologous recombination inhibition in HCC cells.

(A) GSEA of DNA damage response in RNA-seq data from Huh7 cells treated with oxaliplatin (10 μM, left) or adavosertib (500 nM, right) for 24 hours. (B) Western blot analysis of DNA damage-related proteins in the SNU449 and Huh7 cells with indicated treatments for 24 hours. (C) Representative comet assay images from SNU449 and Huh7 cells with indicated treatments (left). DNA in the tail of each treatment group was analyzed (right). n = 50 cells per cell line and condition.

(D) Immunofluorescence analyzed levels of γ H2AX (red; DNA double-stranded break marker). Representative images are shown and the percentage of γ H2AX-positive cells is plotted. (E) Western blot analysis of DNA damage-related proteins in the SNU449 and Huh7 cells with indicated treatments for 24 hours. (F) Heatmap of genes related to DNA_REPAIR in RNA-seq data from Huh7 cells with indicated treatment. (G) The pDR-GFP reporter system was adapted to evaluate the HR function in both Huh7 and SNU449 cells. GFP-positive cells were normalized by flow cytometry (n = 3 per group). (H) Western blot analysis of HR-related proteins in the SNU449 and Huh7 cells with indicated treatments. (I) The pimeJ5-GFP reporter system was adapted to evaluate the NHEJ function in both Huh7 and SNU449 cells (n = 3 per group). The proportion of GFP-positive cells was determined using flow cytometry. (J) Western blot analysis of NHEJ-related proteins in the SNU449 and Huh7 cells with the indicated treatments. (K, L) Representative images of immunofluorescence staining of RAD51 foci (green) or 53BP1 foci (green) and γ H2AX (red) were conducted for HR or NHEJ repair activity, respectively. Scale bar, 5 μ m. Data are represented as the mean \pm SD. *P < 0.05, **P < 0.01 and ***P < 0.001.

Figure 5

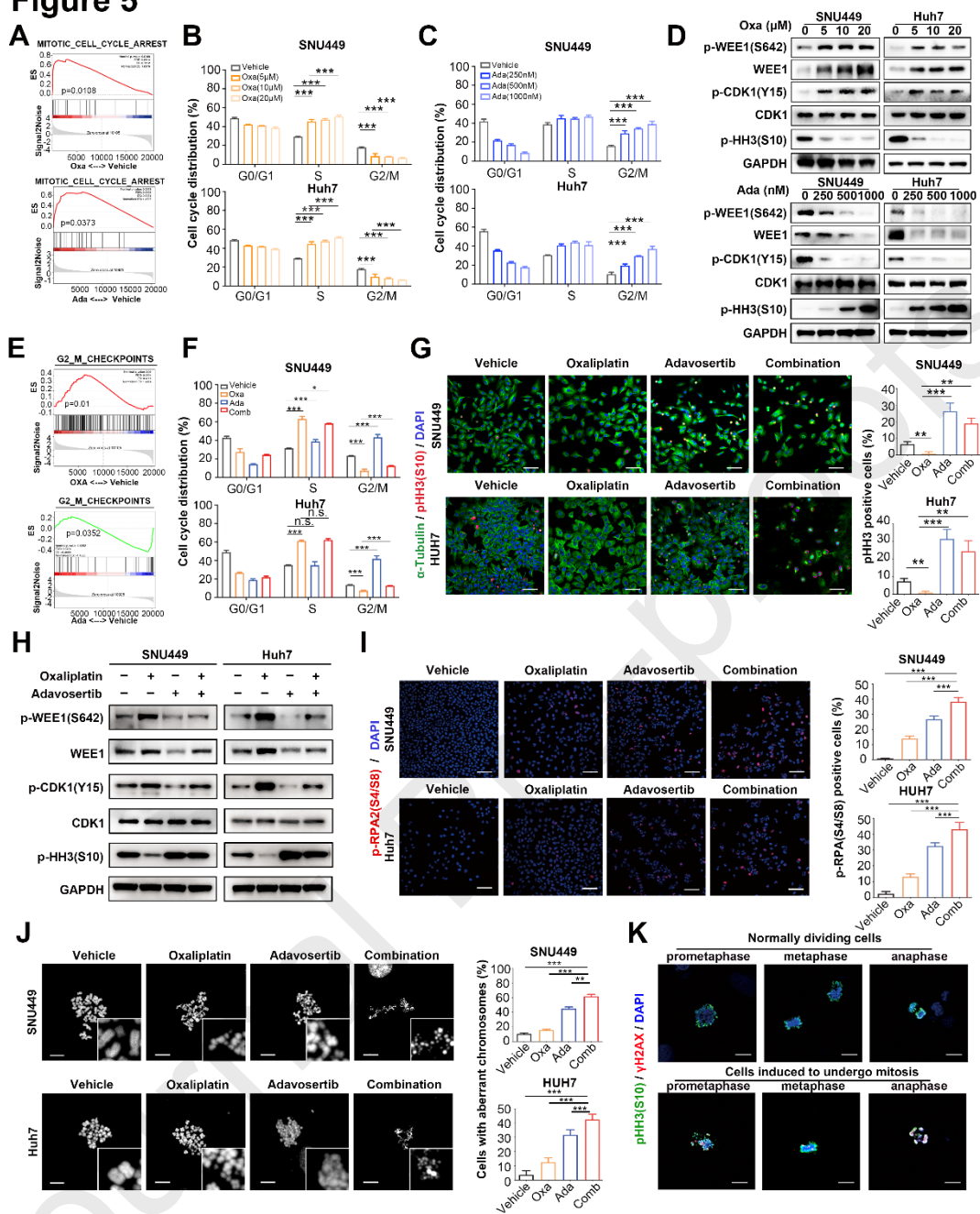


Figure 5. The combination of adavosertib and oxaliplatin disrupts the cell cycle and accumulates replication stress.

(A) GSEA results of cell cycle arrest from the sequence data from Huh7 cells treated with oxaliplatin (10 μ M, left) or adavosertib (500 nM, right) for 24 hours. (B) Flow cytometry was used to analyze the cell cycle distribution of SNU449 and Huh7 cells treated with different concentrations of drug or oxaliplatin (5 μ M, 10 μ M, 20 μ M). The relative quantifications are presented (n = 3 per group). (C) The relative quantifications of cell cycles of SNU449 and Huh7 cells treated with vehicle or

adavosertib (250 nM, 500 nM, 1000 nM) were analyzed by FACS (n = 3 per group). (D) Western blot analysis of G2/M checkpoint-related proteins in the SNU449 and Huh7 cells with indicated treatments for 24 hours. (E) GSEA results of G2/M checkpoint-related pathways in sequence data from Huh7 cells treated with oxaliplatin (10 μ M) for 24 hours. (F) Cells with indicated treatments were assessed for the cell cycle distribution of SNU449 (top) and Huh7 (bottom) cells by FACS analysis (n = 3 per group). (G) Percentage of pHH3-positive (M phase-specific marker) cells in the indicated cell lines. Fields were captured randomly, counting DAPI-positive cells over at least 300 cells (n = 3 per group). Scale bars, 50 μ m. (H) Western blot analysis of G2/M checkpoints-related proteins in cells with indicated treatments for 24 hours. (I) Levels of p-RPA2 (S4/S8) were analyzed by immunofluorescence. Representative images are shown (left) with a scale bar of 50 μ m. The percentage of p-RPA2(S4/S8)-positive cells is plotted (right). Fields were captured randomly, counting DAPI-positive cells over at least 300 cells (n = 3 per group). Scale bars, 50 μ m. (J) Representative images of metaphase spreads are shown (left). A total of 50 metaphases were analyzed from each group. Chromosomal abnormal proportions under each condition are plotted (right). The scale bar is 5 μ m. (K) Representative images of DNA damage at different stages of mitosis were shown by co-staining with anti-pHH3 (S10; Green), anti- γ H2AX (Red), and DAPI (Blue). Scale bars, 5 μ m. Data are shown as mean \pm SD. ***P < 0.001; **P < 0.01; *P < 0.05; n.s., not significant.

Figure 6

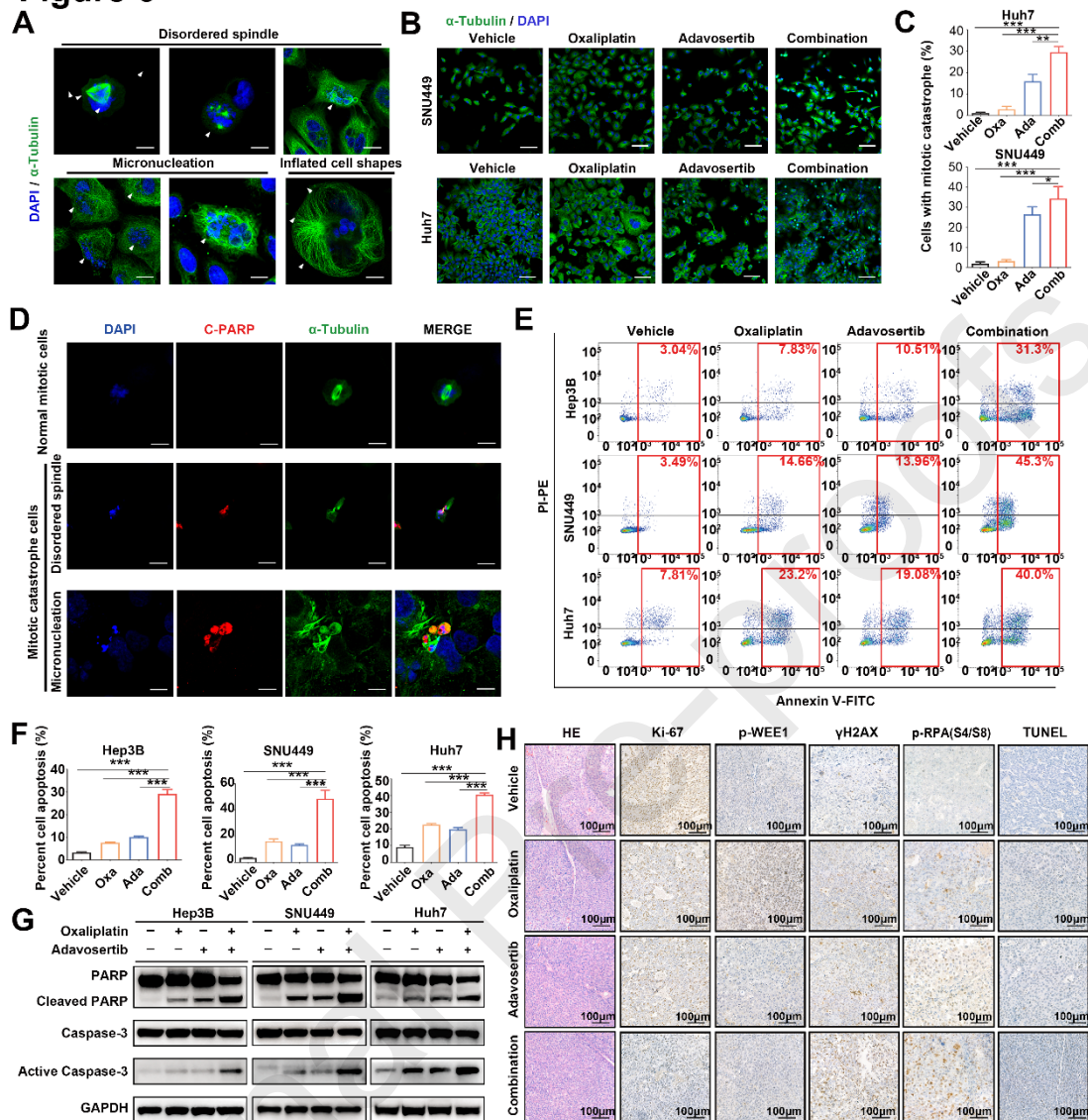


Figure 6. The combination of adavosertib and oxaliplatin induces mitotic catastrophe and apoptosis.

(A) Representative images of mitotic catastrophe cells. Scale bar: 5 μ m. (B) Representative images of the morphology of cells with indicated treatments were captured by confocal microscopy. The scale bar is 50 μ m. (C) The percentage of mitotic catastrophe cells under each condition is plotted. Fields were captured randomly, counting DAPI-positive cells over at least 300 cells each group. (D) Representative images of mitotic catastrophe cells expressing apoptotic signals by immunofluorescence staining with C-PARP (red). Scale bar: 5 μ m. (E) Representative images of cell apoptosis analysis by FACS in the indicated treatments for 48 hours. (F) The relative quantifications of cell apoptosis analysis by FACS in the indicated treatments for 72 hours (n = 3

per group). (G) Western blot analysis of apoptosis-related proteins in cells with indicated treatments for 72 hours. (H) HE, IHC, and TUNEL staining results in the indicated treatments from the subcutaneous HCC xenograft model. Scale bars, 100 μ m. Data are represented as the mean \pm SD. * $p < 0.05$, ** $p < 0.01$, *** $p < 0.001$.

Journal Pre-proofs

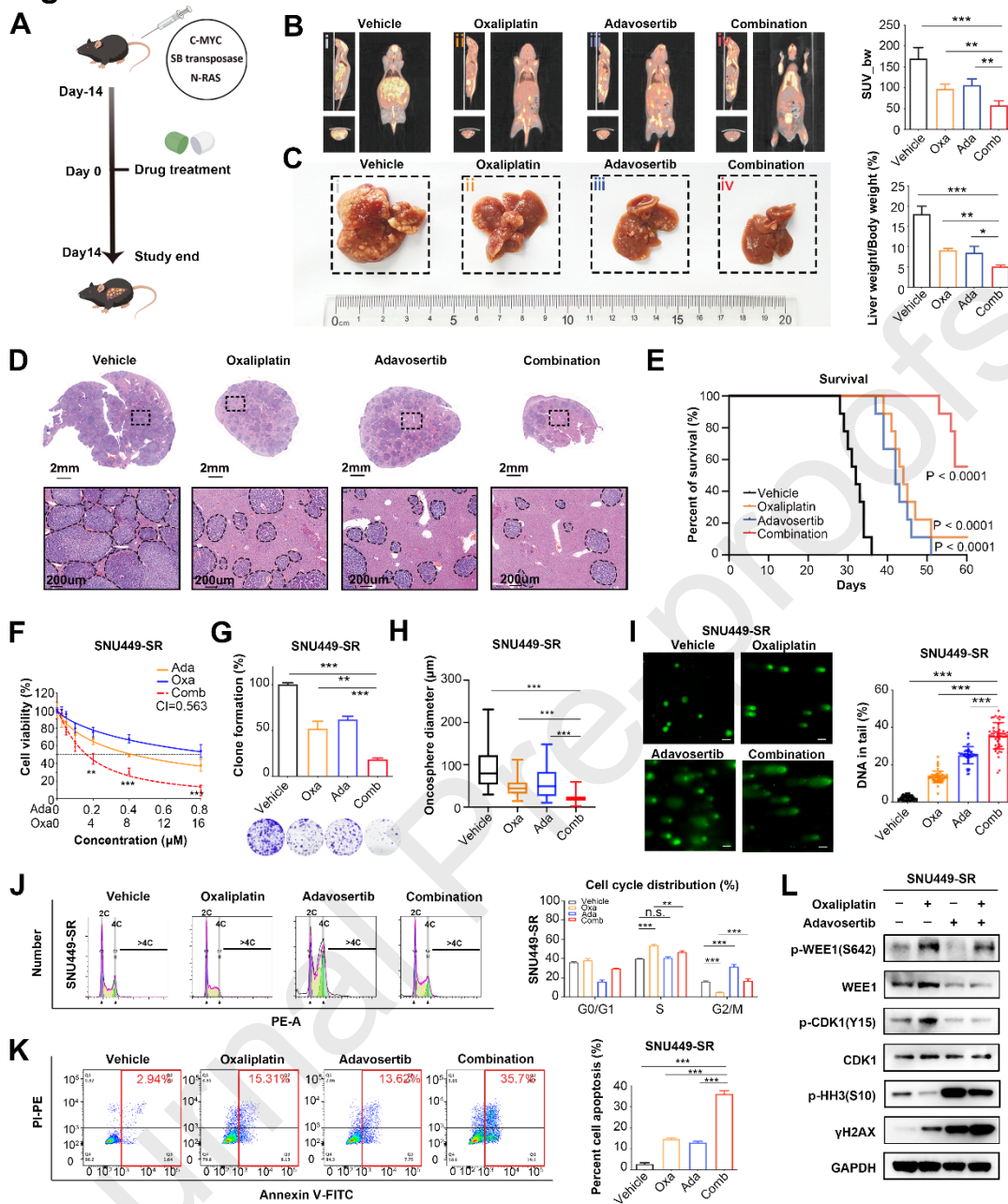
Figure 7

Figure 7. The combination of adavosertib and oxaliplatin shows synergistic tumor suppression effect in HDI models and sorafenib resistant cell lines.

(A) Establishment of the HDI model. (B) PET/CT results and livers of the HDI model with the indicated treatments (n = 3 per group). (C) Representative images of tumor foci from the HDI HCC model (n = 3 per group). (D) HE staining of tumor foci from the HDI model. Representative images indicated tumors with black circles. Scale bars indicate 2 mm or 200 μ m. (E) Survival analysis of mice with different treatments in HDI HCC models (n = 10 per group). Log-rank test for adjusting P value. (F) Dose-response curve of the sorafenib-resistant SNU449 (SNU449-SR) cells treated

with adavosertib (blue), oxaliplatin (orange), and adavosertib + oxaliplatin (red), from a 2-day CCK-8 assay (n = 6 per group). (G) Colony formation assays of SNU449-SR cells exposed to oxaliplatin (2 uM) and/or Adavosertib (100 nM). Colonies containing more than 50 cells were counted after 10 days of treatments (n = 3 per group). (H) Oncosphere formation assays were performed on SNU449-SR cells cultured with oxaliplatin (10 uM) and/or adavosertib (500 nM) grown for 7 days. The scale bar is 2 μ m. (I) Representative comet assay images from SNU449-SR cells with indicated treatments (left). DNA in the tail of each treatment group was analyzed (right). n = 50 cells per group. (J) Cells with indicated treatments were assessed for the cell cycle distribution of SNU449-SR cells by FACS analysis (n = 3 per group). (K) The relative quantification of cell apoptosis analysis by FACS in the indicated treatments for 72 hours (n = 3 per group). (L) Western blot analysis of SNU449-SR cells with indicated treatments. Data are represented as the mean \pm SD. *p < 0.05, **p < 0.01, ***p < 0.001.

revealed that a high level of RS in tumor tissues corresponded with a poor prognosis for the patients. *P < 0.05, **P < 0.01 and ***P < 0.001. (B) Histogram showing the distribution of percentage values comparing RS group expression with clinicopathological features in a cohort of 94 HCC patients. (C) Nonrandom distribution of RS group and HR group across three transcriptomics molecular subtypes. (D) The schematic illustrates the use of PDO and PDX models for validating drug sensitivity in patients with different RS levels. (E) Representative images depicting dead/alive cell ratios in HCC-PDOs treated with various drugs for patients 1-5 (n = 6 per group). Scale: 100 μ m. (F) The dead/living cell ratio of HCC-PDOs derived from patients 1 - 5 in response to different drug treatments (n = 6 per group). Data are represented as the mean \pm SD, *P < 0.05, **P < 0.01, and ***P < 0.001. (G, H) Tumor volume (mm^3) of the PDX models derived from high-RS level patients (patient 1, 2) and low-RS level patients (patient 4, 5) were assessed in the vehicle, adavosertib (50 mg/kg), oxaliplatin (10mg/kg), or adavosertib + oxaliplatin treatment groups (n = 5 per group). (I) The schematic of classification and treatment strategies for HCC based on replication stress levels.

Research Highlights

- According to proteomic and transcriptomic analyses, targeted replication stress has great potential as a liver cancer therapy.
- Through unbiased Kinome CRISPR-CAS9 library screening, we identified the combination of WEE1 inhibitors and oxaliplatin as a novel treatment strategy for liver cancer targeting replication stress.
- WEE1 inhibitor adavosertib demonstrated a strong synergistic effect with oxaliplatin in multiple in vivo and in vitro liver cancer models.
- Adavosertib inhibits oxaliplatin-induced homologous recombination repair and G2/M checkpoints, causing chromosomal damage and mitotic catastrophe.
- Replication stress in liver cancer patients can predict prognosis and chemotherapy sensitivity.

Ethics approval and consent to participate

The research conducted in this study adhered to the ethical guidelines outlined in the Declaration of Helsinki. All tissue samples were obtained from patients with liver cancer who underwent surgery at the First Affiliated Hospital of Zhejiang University School of Medicine. Written informed consent was obtained from each patient. This study was approved by the Ethics Committee of the First Affiliated Hospital of Zhejiang University School of Medicine (Ethics Code 2021-384). All animal experiments were approved by the Animal Care Committee of Zhejiang University (Ethics Code 2019-1218) and were conducted in strict accordance with the National Institutes of Health Animal Care and Use Guidelines.

Competing interest Statement

The authors declare that they have no competing interests.